THESIS FOR THE DEGREE OF DOCTOR OF PHILOSOPHY
IN
THERMO AND FLUID DYNAMICS

Active Flow Control for Drag Reduction of Heavy Vehicles

MOHAMMAD EL-ALTI

Division of Fluid Dynamics

Department of Applied Mechanics

CHALMERS UNIVERSITY OF TECHNOLOGY

Göteborg, Sweden, 2012

Active Flow Control for Drag Reduction of Heavy Vehicles

MOHAMMAD EL-ALTI
ISBN 978-91-7385-772-7

Doktorsavhandlingar vid Chalmers tekniska högskola
Ny serie nr 3453
ISSN 0346-718X

Division of Fluid Dynamics
Department of Applied Mechanics
Chalmers University of Technology
SE-412 96 Göteborg, Sweden

Phone: +46-(0)31-7721000
Fax: +46-(0)31-180976

Printed at Chalmers Reproservice
Göteborg, Sweden, 2012

Active Flow Control for Drag Reduction of Heavy Vehicles

Mohammad El-Alti

Division of Fluid Dynamics
Department of Applied Mechanics
Chalmers University of Technology
SE-412 96 Göteborg, Sweden

Abstract

This thesis considers the aerodynamics of trucks. The work focuses on the aerodynamic drag caused by the wake. Bluff-body flows are dominated by large dissipative vortex-shedding wakes with a low mean pressure compared to the high pressure on their frontal area. This induced pressure difference is the major contribution to the total aerodynamic drag. The flow separation at the aft of the trailer results in a large low pressure region that increases the pressure difference between the front and back. An effective way to decrease the size of the separation zone and increase the base pressure is to use active and passive flow control techniques (AFC and PFC).

The objective of the present work is to apply active and passive flow control (AFC) strategies to reduce the typically large base pressure on bluff-bodies. The work is mainly based on numerical computations using large-eddy simulation of the turbulent flow on a simple semi-3D truck model. A thorough parameter study of a novel rear-end trailer geometry and the AFC parameters is carried out and an attempt is made to optimize the flap shape with AFC using Response Surface Methodology. The flow reattachment process, dynamics of the flow with and without AFC and corresponding wake structures are discussed. An experimental investigation of a typical synthetic-jet actuator is also carried out in order to evaluate the order of magnitude of the maximum possible momentum coefficient, C_μ. A semi-detailed $1/10^{th}$ scale of a VOLVO cab with a trailer is experimentally and numerically evaluated with and without AFC. A full-scale road test employing AFC in a full-scale Volvo truck-trailer is also carried out.

Keywords: Bluff-body, Wake, Active and Passive Flow Control, Drag reduction, Trucks, Heavy vehicles, Tilt-rotor wing, Aircrafts, Large-eddy Simulation, Response surface methodology, optimization, Synthetic-jet Actuator, Full-scale road test

List of Publications

This thesis is based on the work contained in the following papers:

I M. El-Alti, P. Kjellgren and L. Davidson, 2008, On the Download Alleviation for the XV-15 Wing by Active Flow Control Using Large-Eddy Simulation, *ERCOFTAC WORKSHOP: Direct and Large-Eddy Simulation 7*, September 8-10, Trieste, Italy

II M. El-Alti, P. Kjellgren and L. Davidson, 2009, Drag Reduction for Trucks by Active Flow Control of the Wake Behind the Trailer, *Turbulence, Heat and Mass Transfer 6*, K. Hanjalic, Y. Nagano and S. Jakirlic (Editors), 2009 Begell House, Inc.

III M. El-Alti, V. Chernoray, P. Kjellgren and L. Davidson, 2009, Experimental Investigation of a Simple Synthetic Jet Actuator for Active Flow Control Purposes, *Internal Report: Applied Mechanics, div. of Fluid Dynamics*, Chalmers University of Technology, March, Gothenburg, Sweden

IV M. El-Alti, V. Chernoray, P. Kjellgren, L. Hjelm and L. Davidson, 2010, Computations and full-scale tests of active flow control applied on a Volvo truck-trailer, *Aerodynamics of Heavy Vehicles III: Trucks, Buses and Trains*, Potsdam, Germany, 12-17 September

V M. El-Alti, V. Chernoray, M. Jahanmiri and L. Davidson, 2012, Experimental and Computational Studies of Active Flow Control on a Model Truck-Trailer, *European Physics Journal - Web of Conferences*, Volume 25, No. 01012

VI M. El-Alti, P. Kjellgren and L. Davidson, 2012, Shape optimization and active flow control of truck-trailers for improved aerodynamics using Large-Eddy Simulation and Response Surfaces, *to be submitted to scientific journal*

VII M. El-Alti, P. Kjellgren and L. Davidson, 2012, On the numerical modeling of active flow control for aerodynamics applications and its impact on the pressure field, *to be submitted to scientific journal*

Division of work between the authors

The respondent is the first author of all papers on which this thesis is based. Analysis work presented in this thesis was carried out in discussion with supervisor Lars Davidson, who provided valuable comments and revised all papers and the manuscript. The respondent produced all results, except Paper V, in which the numerical analysis was performed by the respondent and the experimental work was performed by co-author Valery Chernoray. This was a project carried out as a bachelor thesis supervised by the authors. In paper IV, the electrical installation was performed by Lars Jernqvist and the full-scale trailer add-on was built by Specialkarosser AB, headed by Bengt Karlsson. The majority of the numerical simulations were carried out using in-house code, developed by co-supervisor Per Kjellgren who provided valuable comments to the work and support of the code.

Other relevant publications

I P. Kjellgren, M. El-Alti and L. Davidson, 2009, Download Alleviation of a Tilt-rotor Wing by Active Flow Control Strategies, *KATnet II Conference: Key Aerodynamic Technologies*, May 12-14, Bremen, Germany

II Mohammad. El-Alti, 2009, Active Flow Control for Aircrafts and Heavy Vehicles, *Thesis for Licentiate of Engineering no. 2009:011*, Applied Mechanics, div. of Fluid Dynamics, Chalmers University of Technology, Göteborg, Sweden

Acknowledgments

The present work was conducted at the Division of Fluid Dynamics, Department of Applied Mechanics, Chalmers University of Technology. The first part of the research presented in the thesis has been a part of the “Gröna bilen” program, which is financed by the Swedish Agency for Innovation System (VINNOVA) and the Swedish Energy Agency (Energimyndigheten). The second part of the research has been a part of the “Fordonsstrategisk forskning och innovation” program which is financed by Energimyndigheten. The work was supported by VOLVO 3P, Specialkarosser AB and Per Kjellgren Engineering. Financial support by SNIC (the Swedish National Infrastructure for Computing) for computer time at C3SE (Chalmers Centre for Computational Science and Engineering) is gratefully acknowledged.

I would like to take this opportunity to thank God for his guidance and all people who have been of great help during the course of this work.

First and foremost, my deep and sincere gratitude goes to my supervisors, Professor Lars Davidson and Per Kjellgren, for their support, guidance and constant source of motivation. Your enlightening discussions and brilliant advice have made this work possible. You shared your profound knowledge in active flow control and CFD with me.

I would like to thank Linus Hjelm at VOLVO 3P and Bengt Karlsson at Specialkarosser AB for your valuable advice and all the interesting discussions during the status meetings. Thanks also to Zenitha Chronéer at VOLVO 3P and Fred Ross at CD-ADAPCO for sharing some STAR-CCM+ knowledge with me. Thanks also to Lars Jernqvist for all electrical expertise solutions to prepare the full-scale test. Elsbeth Mosedale and the rest of CD-ADAPCO’s support team, thanks for your valuable support and solving my STAR-CD problems. Special thanks to all (ex)colleagues and staff at the Division of Fluid Dynamics for the friendly and stimulating environment, especially Valery Chernoray for interesting experimental collaboration and Abdallah Abou-Touk, Mohammad Irannezhad and Prof. Sinisa Krajnović for all your help and interesting discussions.

I express warmest and deepest gratitude to my family, my mother

Souad and father Imad who always encouraged me to higher education, my bothers Mahmoud and Ahmed, my sister Zeina, my beloved wife Warde, my son Mahmoud and my daughter Souad for all your love and support. Thanks also to my aunt Hala for your support.

Nomenclature

Upper-case Roman

C_D	Aerodynamic drag coefficient
C_L	Aerodynamic lift coefficient
$C_R,\ C_I$	Smagorinsky model coefficients
C_s	Smagorinsky model coefficients
C_μ	Momentum coefficient
F^+	Non-dimensional frequency
Kn	Knudsen number
Pr	Prandtl number
Ma	Mach number
Re	Reynolds number
S_{ij}	strain rate tensor
St	Strouhal number $(St = (fD_j)/U_j)$
T	Temperature
U_∞	Free stream velocity

Lower-case Roman

c	Wing chord
e	Energy
f	Frequency
f_i	Body force
k	kinetic energy
p	pressure
t	time
v_i	Cartesian components of velocity vector
u	streamwise velocity component
v	wall-normal velocity component
w	spanwise velocity component
w	width of the truck-trailer
x_i	Cartesian coordinate vector component

Upper-case Greek

Δ	filter width

Lower-case Greek

δ_{ij}	Kronecker delta
ε_ν	viscous dissipation
α	Flap angle
β	Slot angle
μ	Dynamic viscosity
ν	kinematic viscosity $(\nu = \mu/\rho)$
ρ	density
σ_{ij}	stress tensor
τ_{ij}^{SGS}	viscous tensor

Subscripts

∞	free stream or ambient conditions

Superscripts

SGS	subgrid scale
$\sim$	Favre filtered quantity
$-$	spatially filtered quantity
$''$	unresolved quantity
$'$	resolved fluctuation

Symbols

$\langle \dots \rangle_t$	time averaged quantity

Abbreviations

AFC	Active Flow Control
CFD	Computational Fluid Dynamics
CFL	Courant-Friedrichs-Lewy
DES	Detached Eddy Simulation
DNS	Direct Numerical Simulation
LES	Large Eddy Simulation
OFM	Overall Figure of Measure
PFC	Passive Flow Control

RANS	Reynolds Averaged Navier-Stokes
RSM	Response Surface Methodology
ZNMF	Zero Net Mass Flux

Contents

Chapter 1

Introduction

1.1 Background

ENVIROMENTAL requirements are becoming stricter, the international competition in the heavy vehicle industry is even harder during these times of financial turbulence, fuel prices are still increasing and the energy resources of the world are decreasing. The so-called Arab Spring affected oil and gas supplies, e.g. the temporally loss of the Libyan supply. The tragic Fukushima accident in Japan had harsh effects on nuclear and other energy sources around the world. The global energy consumption growth is 2.5%, which is in line with the historical average but well below the 5.1% in 2010. Emerging economies accounted for all of the net growth, China alone accounted for 71% of the growth in energy consumption, (Petroleum, 2012). Fuel prices and energy consumption are expected to increase continuously in the near future.

The global warming problem caused by greenhouse gas emissions is among the hottest political debate questions around the world. Carbon dioxide (CO_2), nitrous oxide (NO_x) and particulate matter (PM) are believed to be the main exhaust emissions that pollute and contribute to global warming. By 2050, EU must reduce emissions in the transport sector by 60% compared to 1990 levels to achive a limit in global warming to $2^{\circ}C$. EU needs to reduce its emissions by $80 - 95\%$ by 2050 in order to achieve this goal, (EU, 2012).

The aerodynamics of today's trucks is far from optimal. Truck-trailers typically have a rectangular geometry on the rear-end with four perpendicular corners. This shape is mainly an effect of practical issues in transporting goods because the desire is to maximize the load capacity. There are also regulations in EU that limit the total length of truck-trailer combinations. The maximum permitted length

of the truck in EU is $18.75m$. The dimensions of the trailer have been optimized according to these regulations. Cooperation between truck and trailer companies regarding aerodynamics to improve the overall aerodynamics of truck-trailers has not had a high priority. The present thesis is supported by both a truck and a trailer company in order to bring about closer cooperation. To develop more environmentally friendly vehicles to meet the growing environmental requirements, the harder international competition in the heavy vehicle industry and the ever increasing fuel prices, the trailer must be considered in the aerodynamic design development, (Hjelm & Bergqvist, 2007).

1.2 Motivation

This thesis presents research on improvements in heavy vehicle aerodynamics improvements to reduce fuel consumption and improve environmental performance. The aerodynamic drag is the major energy loss at highway cruising speeds and the base drag is the dominant contribution to the total aerodynamic drag. Most of the drag on a truck is caused by the wake behind the trailer, which is called the base drag. It is caused by the sharp edges on the rear end where the flow naturally separates. This effect gives rise to a large low pressure region that increases the pressure difference between the front and back. The large low pressure region is a force that acts backwards, opposite to the truck direction. An effective way to increase the pressure on the back is by introducing angled flaps. By introducing the flaps at an angle less than the natural separation angle, the wake becomes narrower, and this decreases the base drag. If the angle is increased, the base drag increases. The idea is now to further decrease the base drag by attaching the flow onto the flap surface. The re-attachment is done using active flow control (AFC). The flaps on trailers are not load bearing.

The idea of using flaps and re-attaching the separated flow is in line with successful research on tilt-rotor aircrafts, (El-Alti *et al.*, 2008; Kjellgren *et al.*, 2009), that was a continuation of previous research, (Kjellgren *et al.*, 2000, 2002*b*; Darabi & Wygnanski, 2004).

1.3 Objectives of the Thesis

The focus is on reducing aerodynamic drag by using active and passive flow control strategies. The objectives are to:

Evaluate possible drag reduction of trucks without changing the trailer geometry. How much drag reduction can be achieved if trailer add-on devices are considered? Basically, when the drag of a truck is reduced, its cargo room must remain unaffected because of restrictions in shape for cargo space and regulations. The remaining freedom is in the design of the front end (cab) or mounting add-on devices. The scope of this thesis is evaluation of mounted add-on devices on the rear end of the trailer.

Investigate active flow control techniques using numerical simulations (LES) applied to simplified truck models. How does the flow field look with and without AFC? What are the main flow features or flow improvements related to AFC? How is the wake affected?

Relate LES computations with full-scale vehicle road tests and experiments on scale models. Is there repeatability of the drag reduction? This includes manufacturing of an actuator that is integrated into add-on devices, both for full-scale road tests and for experimental scale models.

Explore the potential of shape optimization of add-on devices, adopting a suitable optimization approach. Is a curved flap more beneficial than a straight one or is a more sophisticated shape the most optimal for aerodynamics properties? This includes defining appropriate geometrical parametrization. The objective is minimal drag and appropriate constraints are set on the different parameters.

1.4 Vehicle Aerodynamics

The aerodynamics of vehicles is a major consideration and is of great importance in vehicle development. Several books or reviews have been written in this field, e.g. (Barnard, 2001) and (Hucho, 1998). It is a critical part of vehicle manufacturing where many efforts, computations and wind tunnel experiments are carried out in order to improve and optimize vehicle aerodynamics. The directional stability of the vehicle,

soiling of headlights, windows and body, noise, cooling of engine, gearbox, brakes and ventilation, air conditioning and, last but not least, fuel consumption are dependent mainly on the flow field around and through the vehicle. In this thesis the aerodynamics related to drag reduction and fuel consumption is the main subject of consideration.

Vehicle aerodynamics was originally inspired by the aerodynamics of airplanes. Ship and airplane designers were inspired by nature, e.g. fish and birds; they copied these natural shapes and their essential features. There is nothing in nature that could inspire vehicle designers; they were inspired by the shapes of ships and airplanes instead. Aerodynamics is of much more importance for airplanes than vehicles. The plane has to produce lift in order to be an airplane. Vehicle aerodynamics is yet dominated by trial and error. However aerodynamics is not the major target when vehicles are designed, with the exception of racing cars. Beside vehicle aerodynamics, the design must be functional, economic and basically look good. Vehicle aerodynamics considerations are consequences of the shape of the vehicle, not the main reason for it.

In general, the flow over a vehicle is fully 3D and resembles bluff-body flows, which are dominated by large dissipative vortex-shedding turbulent wakes that may interact with longitudinal vortices shed from the rear end. The flow in the separated region (wake) is unsteady. The kinetic energy of the vortex-dominated wake is dissipated by turbulent mixing and transformed into frictional heat. This yields the total pressure loss, i.e. low mean base pressure compared to the high pressure on their frontal area, and frequent flow separations when an adverse pressure gradient is too severe. This is due to the loss of momentum near the wall, where separation may be followed by re-attachments. The turbulent boundary layer grows a great deal on heavy vehicles due to their length and the boundary layer at the end of a trailer is extremely thick and unable to overcome any adverse pressure gradient on the flap surface.

1.4.1 Drag

Drag is commonly associated with the non-dimensional number C_D. This number has recently received very strong focus and is perhaps a synonym for vehicle aerodynamics similar to the way that the compression ratio is for combustion engines. The vehicle performance, fuel economy and low emissions are basic properties of a vehicle in which all are dominated by the aerodynamic drag. The total aerodynamic drag is the sum of skin friction and pressure drag. In a viscous fluid, the velocity gradient $\partial u/\partial y$ at the wall is a consequence of the no-slip con-

dition; the flow velocity is zero at walls. This yields molecular friction and induces shear stress which acts on the surface of the body. The resulting force is derived from the integration of the corresponding force component in the free-stream direction as

$$D_f = \int \tau_w \, dS \tag{1.1}$$

which is skin friction drag. On the rear end of blunt bodies there is a strong adverse pressure gradient that induces flow separation in viscous flow. This is related to the pressure drag (or form drag) defined as

$$D_p = \int (p - p_\infty) \sin\alpha \, dS. \tag{1.2}$$

where α is the incidence angle of the pressure force. The total drag is

$$D_{tot} = D_f + D_p \tag{1.3}$$

In order to report the drag force without a dependence on the actual dimensions, the drag coefficient C_D is defined as

$$C_D = \frac{D}{\frac{1}{2}\rho U_\infty^2 A} \tag{1.4}$$

where D is the drag force, ρ is the air density, U_∞ is the free-stream velocity and A is the stream-wise projected area. C_D can be seen as the ratio of the induced drag force of the vehicle to the force of the free-stream dynamic pressure and projected frontal area. The lower the induced force, the lower the C_D. Passenger cars have a drag value around $0.25 - 0.35$, which is about half of the values for truck-trailers that have $C_D = 0.5 - 0.7$. The main difference that contributes most to the drag force of heavy vehicles is the considerably larger projected area as compared to passenger cars. The frontal area of heavy trucks is at least four times larger than that of passenger cars.

1.5 Flow control

Flow control is an active research area in fluid mechanics. Being able to manipulate a flow field in order to achieve desired engineering results seems to be the way to meet today's demands in competitive and efficient solutions for the automotive industry.

> "The process or operation by which certain characteristics of a given flow are manipulated in such a way as to achieve improvements of a specific technical performance."(Fiedler (Gad-El-Hak & Pollard, 1998)).

This definition gives a good description of the field of flow control. Today, the demands for environmental friendly, economical and efficient vehicles are the driving forces for the developments in this active field. The birth of this field scientifically goes back to 1904 when Prandtl presented his work "On Fluid Motion with Very Small Friction" at the Third International Congress of Mathematicians held in Heidelberg, Germany. The boundary layer theory was introduced, where it was controlled actively by suction in order to delay separation on a surface of a cylinder. Advancements in this field were rapid during the Second World War and the Cold War. The need for efficient, competitive and fast aircraft, missiles and other military equipment that include fluid dynamics could not be met without the use of flow control strategies. Some of the advancements include delaying transition in laminar flows to achieve drag reduction. Civilian interest in flow control grew in connection with the energy crisis of 1973 when the goal was to conserve energy by e.g. reducing drag for civilian air, sea and land vehicles. Using computational fluid dynamics, more applications of flow control have been investigated to achieve optimal design targets. This includes reactive control strategies and the developments of micro electromechanical systems (MEMS), (Gad-El-Hak, 2000). Gad-El-Hak (2000) is a comprehensive review of active flow control strategies. Collis *et al.* (2004) and Greenblatt & Wygnanski (2000) review control of flow separation by oscillatory control.

There are different views as to how to classify flow control strategies, (Gad-El-Hak, 2000). The most common is by considering the energy input into the system, as is shown in Figure 1.1(a). If no energy is used while controlling the flow, the flow control is passive, when energy is used, the flow control becomes active.

1.5.1 Passive and Active Flow Control

Passive flow control is achieved by geometrical modifications or additional geometrical configurations in order to control the flow or to generate a desired behavior. A vortex generator is a typical example of passive flow control where a small vane creates a vortex. It is used on airplanes to delay separation at the cost of increasing the frictional drag. The introduction of flaps (figure 3.1(b)) in the present work is a

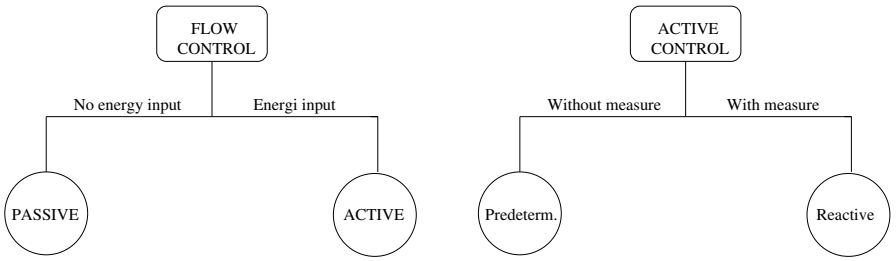

(a) Classification of flow control.

(b) Classification of active flow control.

Figure 1.1: Classification diagram of flow control methods.

kind of passive flow control; the idea is to narrow the size of the wake by maintaining the flow re-attached on the flap surface.

Active flow control is further classified into predetermined and reactive control. The predetermined case is also called open-loop active flow control. Here, predetermined energy is used as input without measuring any quantity in the flow field. A typical device is an actuator with a mechanical motion to control the flow. The effect is linear or periodic excitation of flow in desired regions. Figure 1.1(b) shows this classification. Reactive flow control is when the state of a variable is measured and used in the control process. Reactive flow control can be divided into two cases depending on which variable is measured. If the measured variable is also the controlled one, the reactive control is a closed feedback loop control; otherwise, it is an open feed-forward one.

In this work, predetermined active flow control is used. This choice is based on several basic principles. It is much easier to start an investigation by predetermined control. If there is a net effect, feedback control can be the next step to further improve the flow control. We also assume that trucks are generally driven at a constant speed on highways, in Sweden around $90\ km/h$. Thus there is less need to have feedback control if the truck velocity is constant. However, the weather (e.g. side winds) will probably affect the desired control, although such considerations are presently beyond the scope of this work. Future work will probably include such investigations.

The engineering end results, e.g drag reduction or reducing noise levels, is a consequence of the strategies for controlling the flow. Flow control is used to delay or advance transition, prevent or provoke separation and suppress or enhance turbulence. In this work, flow control is used to enhance turbulence on the flap surface, which in turn delays the separation and finally reduces the size of the wake and the level of turbulence in the wake. It is not always obvious which strategy should

be used in order to control the flow. There are always side-effects that must be dealt with to attain the desired result. The actuators will e.g. increase the level of noise, which could be disturbing for passenger cars behind the truck; the truck driver will probably not hear the increased noise level since the length of the truck is over $13m$.

1.5.2 Other efforts to reduce base drag on trucks

Choi *et al.* (2008) reviewed the most frequent used PFC and AFC strategies to control the flow over a bluff body. Several efforts have been made to minimize the base drag on trucks, both pure passive and combined with active flow control strategies. The investigations in (Pankajakshan *et al.*, 2007) and (Leuchen & Cooper, 2007) both used passive devices mounted at the rear end of the trailer. In (Pankajakshan *et al.*, 2007) and (Hyams *et al.*, 2011) a drag reduction of 15% was achieved by using base flaps inclined, at a 15° and a similar drag reduction was achieved in (McCallen *et al.*, 2004) but at an inclined flap angle of 20°. Leuchen & Cooper (2007) tried vortex generators, base flaps and boattail. The vortex generators actually increased the drag, but the flaps and boattail showed marginal drag reduction. Doyle *et al.* (2008) used the generic algorithm to optimize flaps on 2D trucks. They reported that the drag reduction was high.

Several active flow control efforts have been made, both with and without flaps. Seifert *et al.* (2007) and Henning & King (2005) investigated the case without flaps, Seifert *et al.* (2007) used a circular cylinder that had a built-in actuator and achieved a drag reduction of 20%. Henning & King (2005) used closed-loop control on a blunt trailing edge and got a 10% drag reduction. Taubert & Wygnanski (2007) and Nayeri *et al.* (2007) used base flaps with AFC and reached a drag reduction below 10%. Active flow control was also imposed on the cab in (Buckley Jr. & Marks, 1979) and (Ortega *et al.*, 2009). One successful effort was (Englar, 2005), which achieved a drag reduction of about 30% using steady blowing. This is a promising result, but the use of steady blowing is energy consuming and the net drag reduction is not that high.

These efforts in mind invite to do a parameter study with optimization and use periodic blowing, which is much more effective than steady blowing with almost the same end results, (Seifert *et al.*, 1993).

Chapter 2

Turbulence, modeling and CFD

TURBULENT flow is encountered almost everywhere in our daily life. It captures our attention when we look at the smoke from cigarettes or the swirl of milk in our steaming coffee and we pray to God to avoid feeling it during flights when the airplane shakes and makes the passengers look terrified. Turbulence is important in many industrial flows, almost all flows in the industry are turbulent, e.g. pipe flows, gas turbines, combustion engines, cyclones. External flow around passenger cars, heavy trucks and airplanes is also turbulent. Turbulence is a state of fluid motion characterized by random, chaotic, three-dimensional vorticity and possess a cascade of coherent structures from large to small scales. Fluid motion is governed by the Navier Stokes equations (2.1 and 2.2), which describe the conservation of mass and momentum for a fluid particle subjected to the continuum approximation. The continuum approximation is only valid for $Kn << 1$, where Kn is the Knudsen number, the ratio of the molecular mean free path length to a representative physical length scale (Panton (2005)). The momentum equation is basically Newton's second law, $ma = F$, applied to a fluid particle.

$$\frac{d\rho}{dt} + \rho\frac{\partial v_i}{\partial x_i} = 0 \tag{2.1}$$

$$\rho\frac{dv_i}{dt} = -\frac{\partial p}{\partial x_i} + \frac{\partial \tau_{ji}}{\partial x_j} + \rho f_i \tag{2.2}$$

where d/dt is the material derivative, taking into consideration the local and convective rates of change ($\partial/\partial t + v_j\partial/\partial x$). The terms on the right hand side of the momentum equation 2.2, represent the forces that act on a fluid particle due to pressure, viscous stresses and body

forces. From the constitutive law for Newtonian viscous fluids (shear stress is a linear function of strain) we have that

$$\sigma_{ij} = -p\delta_{ij} + \mu\left(\frac{\partial v_i}{\partial x_j} + \frac{\partial v_j}{dx_i}\right) - \frac{2}{3}\mu\frac{\partial v_k}{dx_k}\delta_{ij} \tag{2.3}$$

The incompressible formulation of the Navier-Stokes equations is valid when the density of the fluid is weakly dependent on pressure, i.e. $d\rho/dt = \partial\rho/dt + v_i\partial\rho\partial x_i = 0$. This is true for Mach numbers below 0.3. The last term in the right hand side of equation 2.3 vanishes when the flow is incompressible. The solutions of fluid mechanics equations are believed to be deterministic, and perhaps unique due to defined boundary and initial condition although the solutions exhibit randomness (George, 2006).

The flow behind the truck is unsteady, and pulsating (i.e. oscillating) jets are used as forcing. Thus the modeling strategy must be transient. The modeled actuator is very narrow and the excitation velocity is about $50 - 100\%$ of the free-stream velocity. The actuation frequency is much higher than the Strouhal frequency of the wake. Fine resolution both in space and time is thus needed. Therefore, in order to make accurate predictions of the turbulent flow, large-eddy simulation is used. This provides both instantaneous field data and high accuracy. The Reynolds number is $200,000$ based on the width (w) of the truck, which is in the manageable range of LES. The inlet velocity is $U_\infty = 25m/s$ and the truck width is $w = 2.6m$. A higher Reynolds number such as in full-scale flow would have forced us to use a hybrid LES/RANS approach, such as DES.

Following Davidson (2011), the filtered Navier-Stokes equations read

$$\frac{\partial\bar{u}_i}{\partial t} + \frac{\partial}{\partial x_j}\left(\bar{u}_i\bar{u}_j\right) = -\frac{1}{\rho}\frac{\partial\bar{p}}{\partial x_i} + \nu\frac{\partial^2\bar{u}_i}{\partial x_j\partial x_j} - \frac{\partial\tau_{ij}^{SGS}}{\partial x_j} \tag{2.4}$$

where $\tau_{ij}^{SGS} = \overline{u_iu_j} - \bar{u}_i\bar{u}_i$ is the sub-grid scale stresses modeled as

$$\tau_{ij}^{SGS} - 1/3\delta_{ij}\tau_{kk}^{SGS} = -2\nu^{SGS}\bar{s}_{ij} \tag{2.5}$$

where ν^{SGS} is

$$\nu^{SGS} = (C_S f\Delta)^2\sqrt{2\bar{s}_{ij}\bar{s}_{ij}} \tag{2.6}$$

and $\bar{s}_{ij}$ is

$$\bar{s}_{ij} = 1/2\left(\frac{\partial\bar{u}_i}{\partial x_j} + \frac{\partial\bar{u}_j}{\partial x_i}\right) \tag{2.7}$$

The Smagorinsky model (2.5) for the sub-grid scales is used with the Smagorinsky constant $C_S = 0.25$. In the near-wall region ($0.08w$)

the filter width is reduced using the Van Driest damping function.

$$f = 1 - e^{-y^+/A^+} \tag{2.8}$$

where $A^+ = 25$ and y^+ is calculated by searching for the closest distance between a node in the domain and the wall node.

The commercial CFD code FlowPhys ver. 2.0 is used for the computations in this work. It has a semi-implicit, fractional step finite element solver. The temporal discretization is the explicit four-step Runge-Kutta scheme for the convection terms and the Crank-Nicholson method for the diffusion terms. The spatial discretization scheme is the pure central difference (CD).

The time step size was controlled by an adaptive time stepper that kept the max Courant number below 2.0. A check was made every 10^{th} time-step. The number of time steps was typically between $100\,000$ and $200\,000$ and the time step size varied between $10^{-3}w/U_\infty$ and $5.8 \cdot 10^{-4}w/U_\infty$.

The forcing is modeled as a transient velocity inlet and the governing variables are the slot width, the velocity (both magnitude and direction) and the frequency, see figure 2.1. The RMS momentum from the slot is defined as

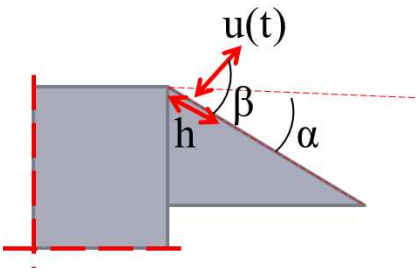

Figure 2.1: The AFC parameters.

$$J_{RMS} = \int \rho u_{RMS}^2 \, dh = \rho u_{RMS}^2 \Delta h \tag{2.9}$$

where Δh is the effective slot width. Further, we define the momentum coefficient as

$$C_{\mu\ RMS} = \frac{J_{RMS}}{w\frac{1}{2}\rho U_\infty^2} = \frac{u_{RMS}^2 \Delta h}{w\frac{1}{2}U_\infty^2} \tag{2.10}$$

From 2.10, the velocity in the slot is given by

$$u_{RMS} = \sqrt{\frac{C_{\mu\ RMS}\ w\ U_\infty^2}{2\Delta h}} \tag{2.11}$$

We further assume that the forcing is purely sinusoidal, i.e.

$$u(t) = \sqrt{2} u_{RMS} \sin(2\pi F t) \tag{2.12}$$

Finally, we define the non-dimensional forcing frequency as

$$F^{+} = \frac{F \cdot X_{TE}}{U_{\infty}} \tag{2.13}$$

where X_{TE} is the distance from the slot to the trailing edge of the flap.

Chapter 3

Research Methods and Models

THIS chapter describes the different research methods used in this thesis. The choice of research method is highly problem dependent and is related to desired types of end-results. The research in this thesis covers all three methods used in aerodynamics research and engineering; numerical simulations (LES and DES), experimental studies and full-scale road test. The rapid increase in computing power over the past two decades made numerical simulations an obvious tool in addition to experimental analysis methods of fluid flow. The ease of simulations depends primarily on its cost-effectiveness for building and testing cycles for evaluation of many designs. Simulations and experiments supplement each other in research and engineering. In this thesis, simulations are used as primarily tool for initial evaluations of a designs or idea. The models are usually considerably simplified, to focus on particular desired end-results and establish basic understanding. Common industrial fluid dynamics problem are governed by a large number of geometrical and system parameters. The initial simplified simulations are mostly used to narrow this wide spectrum of parameters into a manageable number of designs. Simulations also provide immense high resolution field data for analysis of e.g. wake structures or velocity profiles at different positions. Experiments are used to verify and ensure predicted integral quantities which may be supplemented by full scale road tests. Simplified models which increase in complexity as research proceeds resembles the difference between science and engineering perspectives. A scientist focuses on the understanding of a problem at hand and goes to its roots in nature. To do this, scientists removes all side-effects and investigates the very narrow core part of the problem. From this, basic laws of nature are understood and illuminated. On the other hand, engineers uses the

laws of nature, to design a solution that works in the framework of these laws, to understand and predict system behavior. To do this the engineer finds possibilities to determine which laws are important and which can be neglected. This chapter starts with a description of the simplified truck models used in the LES simulations. The models are used to understand and study the effect of AFC and to ensure possibilities of drag reduction on trucks. The simplified truck model is also used to narrow the wide design space and AFC parameters. The experimental model and the indigenous actuator are then described. The chapter ends with a description of the full-scale model used in the road test.

3.1 Simplified truck-trailer models

The truck-trailer is simplified as a rectangular bluff-body with a typical width ($w = 2.6\ m$) and length ($l = 13.0\ m$) relevant for a real truck. The height (z direction) is $h = 0.2\ m$, i.e. the domain is three-dimensional (figure 3.1(b)). The effects of a detailed cab, gap between truck and trailer, wheel housing flow, underbody flow, rear-view mirrors etc. are not studied in this particular model. Some of these details are studied in the experimental model, and all details were included in the full-scale test. The truck is mounted with angled flaps on the rear end in which the oscillating synthetic jet actuators are placed (figure 2.1). The actuators are modeled as a time-varying boundary condition (slot). The slot extends over the entire height (z) of the truck.

The truck geometry is shown in figure 3.1(b). The inlet flow is modeled as the inlet boundary condition (BC) with prescribed constant free-stream velocity, $U_\infty = 25\ m/s$. The outlet BC in FlowPhys is a weak outlet which was prescribed on the outlet boundary and the side walls in the y direction, in the z direction, the side-walls were set to slip BC, see figure 3.1(b). The Reynolds number is reduced to $200\,000$ by increasing the viscosity to $\mu = 3.25 \cdot 10^{-4}$.

The computational mesh is shown in figure 3.2 and 3.3. The number of nodes in the wake and the flap region is very large compared to those in the free-stream region. The mesh size is around $1.4 - 3.3$ million nodes and the mesh consists of unstructured quad elements in the $x - y$ plane which was extruded to 16 hexahedral elements in the spanwise direction. The quality of the mesh was high close to the wall, in particular close to the flap region. Table 3.1 reports the quality of the mesh in terms of y^+, Δx^+ and Δz^+.

Location	y^+	Δx^+	Δz^+
Prior the flap	$1, 0.6$	$20, 15$	$65, 40$
On the flap	$0.3, 0.25$	$5, 5$	$20, 16$

Table 3.1: The quality of the mesh, (max,mean).

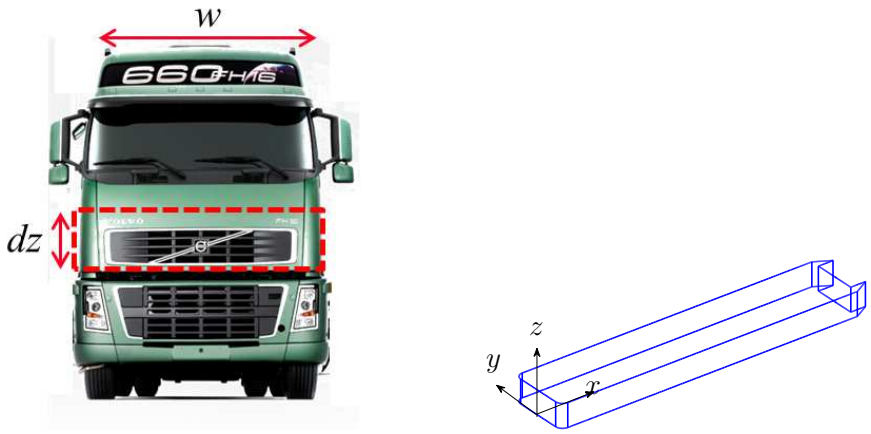

(a) The spanwise slice of the truck.

(b) Simplified truck model.

Figure 3.1: The spanwise slice and the simplified truck model. Inlet at $x = -12w$; outlet at $x = 30w$; side walls at $y = -8.5w$ and $y = 8.5w$.

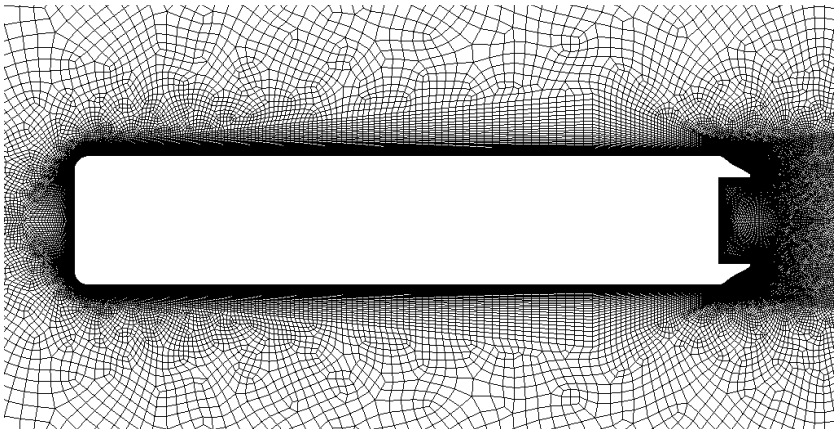

Figure 3.2: 2D slice of the mesh around the truck.

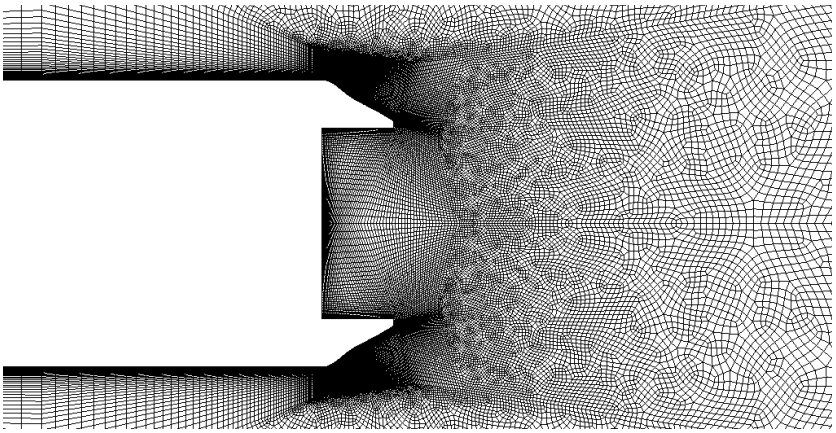

(a) 2D slice of the mesh around the wake region.

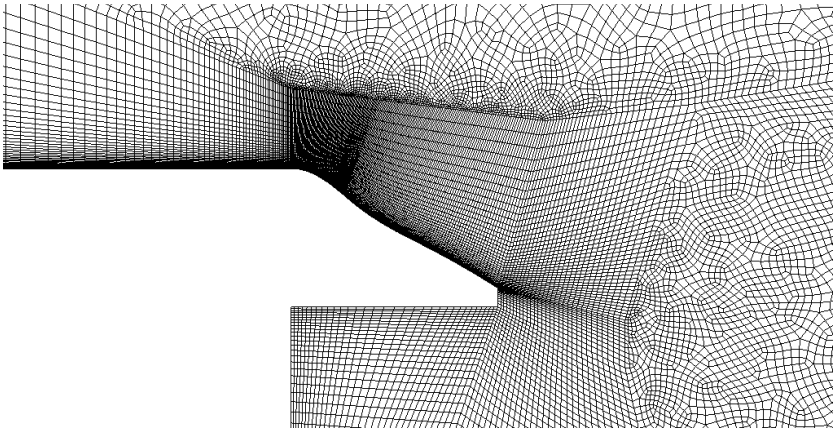

(b) 2D slice of the mesh around the flap region.

Figure 3.3: 2D slice of the straight flap at the rear-end of the trailer, geometry and mesh.

3.2 Experimental Model

The experimental model truck is a $1:10$ scale model of the Volvo FH16 that has a fully detailed cab and simplified underbody and wheel housing; the cooling flow is closed. The trailer has a realistic geometry with a simplified underbody. The model front and rear views are shown in figure 3.4. The CAD model was created in two separate main parts, tractor and trailer. The tractor geometry was simplified using CAE software, ANSA. Much effort was made to make the model well sealed both for the computations and for the SLS rapid prototyping machine. The trailer CAD was drawn in CATIA, which has the possibility to easily construct the flaps and actuation details and to export to ANSA or the SLS machine. Most of the trailer was made of Medium Density Fiberboard (MDF) material, and was not printed in the SLS machine. The flaps and the box-shaped rear end were made to be easily interchangeable as modules connected with rails to the rear end of the trailer. The geometrically complicated parts, such as the flap modules and the tractor, were printed. Three different configurations were studied: a trailer without flaps (baseline case), with flaps (PFC case) and with flaps and AFC (AFC case).

Several transitional ducts were made in the flap modules which guide the flow smoothly from the loudspeaker to the actuator slots, see Figure 3.5. The base pressure is measured via pressure tubes that are connected to integrated pressure channels in the interchangeable modules. The pressure was measured in 12 positions for the baseline case and 16 positions for the PFC/AFC case. The positions are at one half side of the trailer base, assuming symmetry. Figure 3.6 shows the distribution of the pressure locations. For the module with flaps, ten positions are on the flaps surfaces and six are on the trailer base.

Experiments were carried out in a closed circuit wind tunnel with test section dimensions of $3.00x1.80x1.25m^3$ and a speed range of $0 - 60m/s$, see Figure 3.7. The actuator used in the experiments was a synthetic jet actuator based on a loudspeaker enclosed in cavity. The flow actuation was performed through the slots located at the corner of the rear end and flaps. The loudspeaker was mounted inside the trailer, and the flow was guided via the profiled channels (Figure 3.5) in the trailer to the slots at the rear end. During the experiments, the velocity from the actuator slot was measured by a traversing hot-wire probe at the slot outlet. The drag force of the model was measured using an external six-component balance. The base pressure was monitored by a number of pressure taps positioned on the surface of the trailer base and flaps (Figure 3.6). The visualization of the flow separation was performed by surface tufts. The flow Reynolds number was $250\,000$

(a) Front view

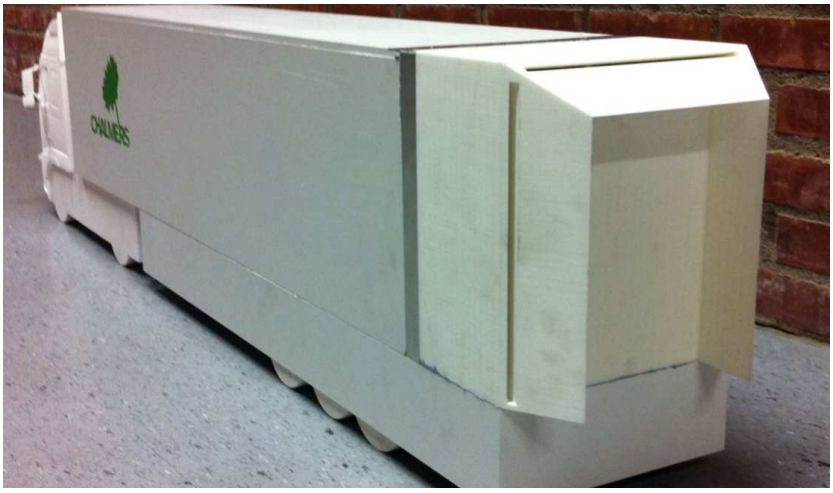

(b) Rear view

Figure 3.4: A front and rear view of a $1:10$ experimental scale model of a VOLVO FH16 with flaps. The slots are shown in the rear view.

in the main series of experiments and a Reynolds number sweep was made from $80\,000$ to $500\,000$ in order to measure the dependency of C_D on the Reynolds number.

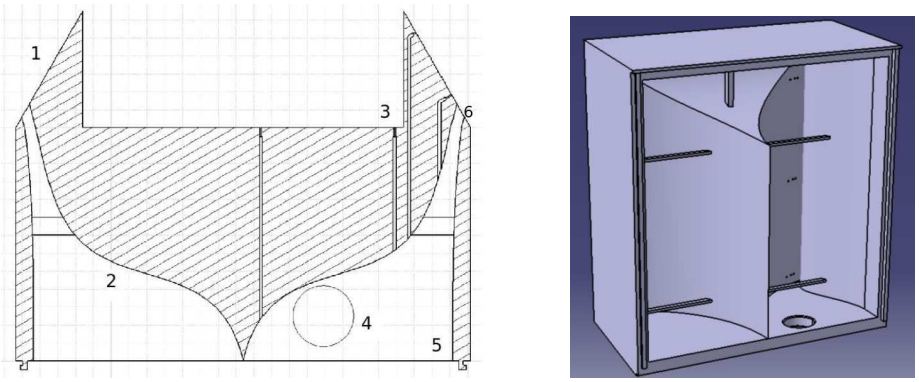

(a) Cross section view of rear end modules (b) CAD of rear end modules

Figure 3.5: A cross section and 3D figure of the interchangeable rear end modules. In the cross section (top view), we can see the flaps (1), the profile channels that guide the air from loudspeaker to the slot on the flap surface (2), the integrated pressure channels in the geometry (3), the exit of the pressure tubes (4), the profile of the rails that connect this module with the trailer (5) and, finally, the AFC slots (6).

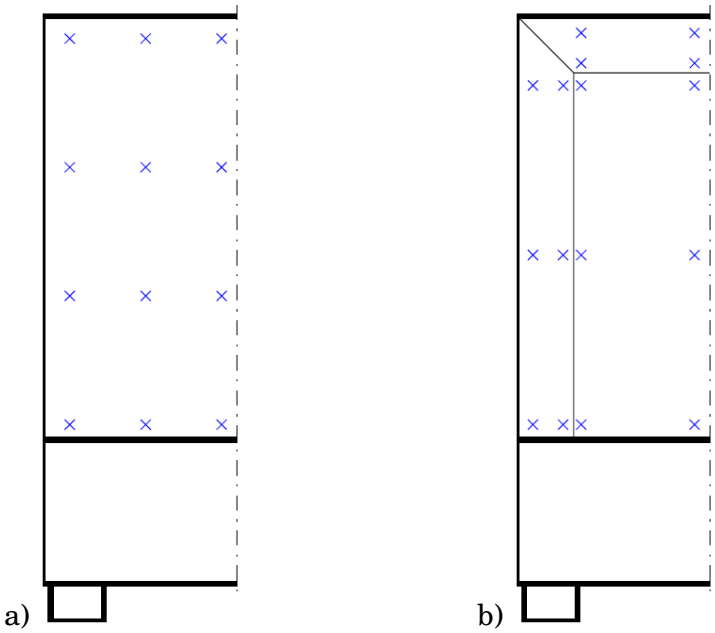

(a) Baseline (b) PFC

Figure 3.6: The locations of the pressure holes for the baseline (a) and PFC/AFC (b) cases.

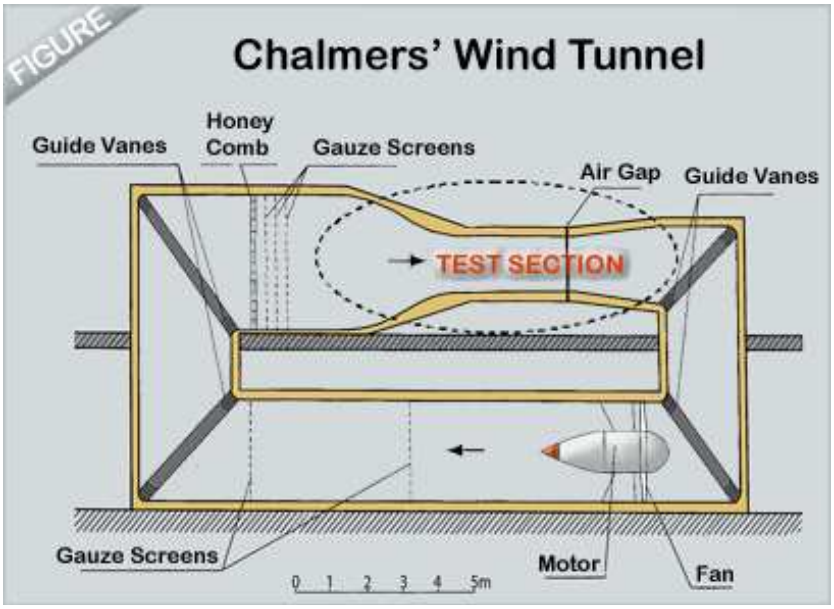

Figure 3.7: The experiment was carried out in Chalmers close circuit wind tunnel

3.3 Synthetic jet actuators

A synthetic jet is produced by subsequent vortices that are formed by oscillating blowing and suction of fluid across a slot such that the net mass flux is zero (ZNMF). The term "synthetic jet" was coined by Glezer & Amitay (2002). The difference between ordinary and synthetic jets is that the latter extracts the fluid from the ambient flow and transfers linear momentum to it without net mass injection across the slot. During the ejection and suction stroke, vortex rings are formed (Smith & Glezer (1998)) and synthetize a jet in a time-averaged context. To make use of this technique, a reliable and sufficiently powerful synthetic jet (also known as zero-mass flux) actuator was evaluated for experimental full-scale tests. There are many sophisticated synthetic jet actuators. Seifert (2007) and Cattafesta & Sheplak (2011) review available actuators for active flow control. A classification from Cattafesta & Sheplak (2011) of the many different actuators based on function is given in figure 3.8.

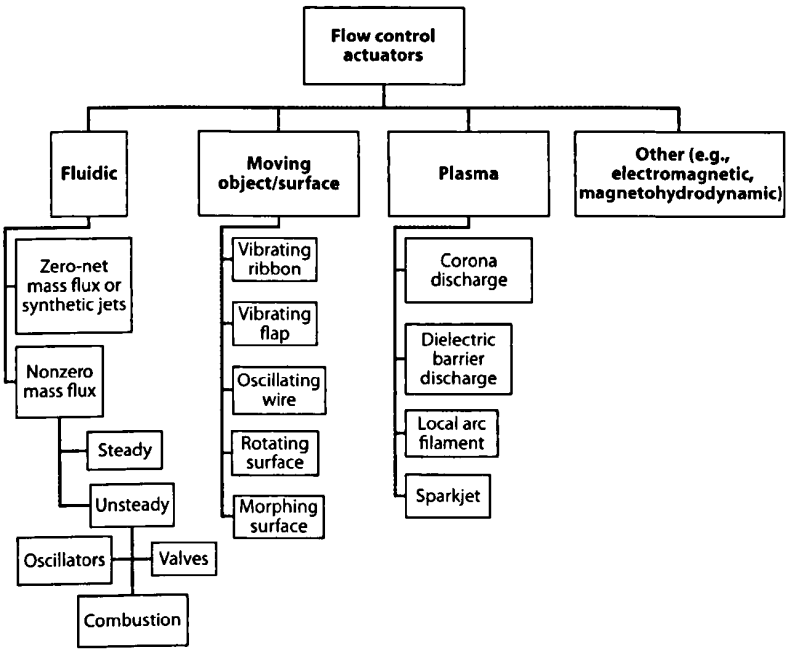

Figure 3.8: An overall classification of different actuators for active flow control, from Cattafesta & Sheplak (2011).

The fluidic types of actuators include the ZNMF and non-zero mass flux actuators. An interesting actuator of the latter type is the suction and oscillatory blowing actuator (SAOB) discussed by Arwatz *et al.*

(2008). The SAOB combines both suction and oscillatory blowing in one device without any moving or active elements. We chose a simple and cost-effective one: a loudspeaker in cavity ZNMF fluidic actuator. The actuator is active when the loudspeaker membrane is set in vibration; the air is compressed out from the slot and produces a sinusoidal synthetic jet. The advantages of this type of actuators is that it does not require any additional or external flow source and it is easily scalable from small scale experiments to full scale tests. The disadvantages are that the peak velocities are limited and are mainly achieved at the resonance frequency of the device. Other disadvantages are high weight due to the magnet and high heated loudspeaker coil for continuous operation. The oscillatory motion of a diaphragm to create ZNMF synthetic jet can be achieved by either piezoelectric or electrodynamic configuration. The choice of the electromagnetic ZNMF actuators is mainly due to their large displacement capabilities which make them attractive in the low frequency domain. Figure 3.9 describes the function of the electromagnetic configuration. The motion of the diaphragm is created by the coil using electrodynamic transduction. The magnet imposes a magnetic field and AC current passes through the coil, which produces an AC electromagnetic force that induces the oscillating motion of the diaphragm around its equilibrium position (Cattafesta & Sheplak (2011)).

The aim is not an optimized and effective actuator with consideration to size, weight, effectiveness (power input) and powerfulness (maximum momentum output) but rather a simple prototype model that can produce enough power and is cost-effective and easy to manufacture for testing purposes. This actuator must be sufficiently powerful in the low frequency domain. Our frequency domain is between 15 and $20Hz$, and the goal is to reach a momentum coefficient of $0.5\% \leq C_\mu \leq 1\%$.

The actuator consists of a rectangular wood cavity ($V_1 = WxLxH = 28.3x28.4x5\ [cm]$), a loudspeaker and an aluminum plate with a slot in the middle. The cavity volume can be adjusted by moving the loudspeaker, i.e. producing different H, see figure 3.10. The actuator was well sealed inside in order to maximize the momentum output.

Seifert (2007) discusses inherent properties of actuator systems and the factors that govern efficiency and robustness. Seifert (2007) discusses the potential of the dimensionless numbers to compare different actuation systems. The overall figure of merit is defined as

$$OFM \equiv \frac{F_a^2 U_p}{W_a P_{act}} \tag{3.1}$$

where F_a is the actuator thrust in fluid at rest, W_a is the weight of the actuator, U_p is the peak velocity and P_{act} is the power consumption.

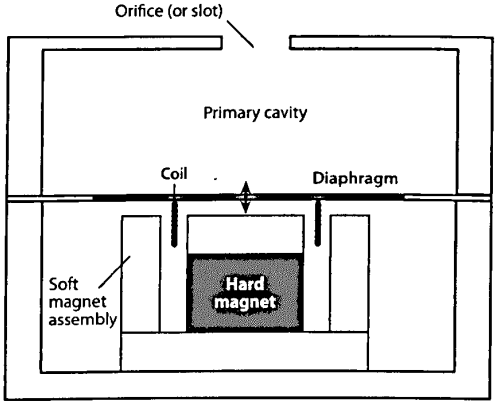

Figure 3.9: Schematic view of the electromagnetic ZNMF actuator, from Cattafesta & Sheplak (2011).

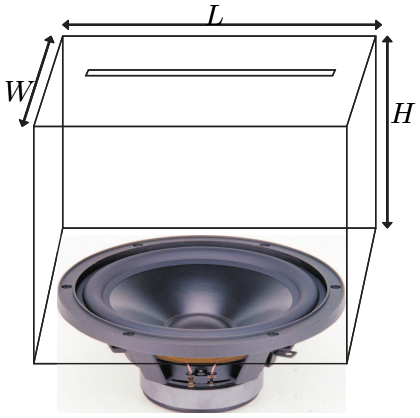

Figure 3.10: Schematic view of the actuator.

3.4 Full-scale road test

The full-scale tests were conducted at the Hällered proving ground in Sweden (figure 3.11), one of the largest proving grounds in Europe ($6.2km$), and was opened 1972 (UKIP, 2012). The main track is oval in shape and is one of 15 tracks for vehicle testing. The fuel consumption was measured at different stages of the road track and was compared for the different cases at Hällered. The "Joint ATA/SAE Fuel Consumption Test Procedure, Type II" was adopted to assure consistency in the tests. This procedure is a standard method for full-scale fuel consumption investigations, (R. Buzz Powell & Rosenthal, 2009). The test vehicle together with a similar reference vehicle are run at the road track, with and without AFC, repeated times in order to minimize the effect of weather and other sources of error. In this test, five runs were carried out with both vehicles for each case. From the differences of the cases of with and without AFC, possible percentage fuel savings are calculated. The operation of the vehicles was synchronized using handheld radios and distance/time tracking in order to ensure identical cycles.

Figure 3.11: Hällered proving ground in Sweden.

3.4.1 Configuration

The Volvo test and reference vehicles were both equipped with cruise control, keeping a constant speed of 90km/h. The vehicles width were $2.6m$ and length $16m$. Both vehicles were equipped with cab spoilers and side air deflectors. Before the test, the vehicles had a full tank and tire pressures were controlled. Three flaps were mounted at the rear end of the test vehicle (figure 3.12(a)). The side flaps had six actuators and the top flap had five (figure 3.12(b)). The actuators were connected to five amplifiers, four actuators/amplifier plus one stand-alone, and the power was obtained from two small power stations located in

the trailer. The frequency and amplitude of the actuation signal were controlled by a LabVIEW program from the truck via WIFI network. The actuation was active only in the two straight paths of the proving ground, and the fuel consumption was reported for this part of the track.

(a) The mounted flaps

(b) The integrated actuators

Figure 3.12: The VOLVO full-scale test vehicle

Chapter 4

Optimization Approach

SURROGATE models are adopted as the optimization approach. The specific model is the polynomial response surface methodology (RSM). The main advantage of this method is that all candidate designs can be run parallel in time. The model does not require information between the candidates during the simulation time. This is very useful when running experiments or heavy CFD computations. This optimization strategy was chosen mainly because it is robust and because the aim is to find a region of feasible designs instead of using the usual gradient-based local minimum/maximum seeking optimization strategies. It is the understanding of the response of each parameter in the system that makes this algorithm useful during physical fluid analysis.

4.1 Response Surface Methodology

The idea of RSM is to build an empirical model of the true response surface of the system. The true response surface is governed by physical laws. The data obtained from the design candidates are used to build a mathematically best fitting model. A second-order polynomial model has been adopted in order to capture non-linearities. The model also includes interaction terms of the different parameters. Following the procedure in (Myers & Montgomery, 2002) the true response is denoted as y, the design parameters $x_1, x_2, x_3, ..., x_n$, then we have the following statement

$$y = f(x_1, x_2, x_3, ..., x_n) + \epsilon \tag{4.1}$$

where ϵ is all sources of errors which can be divided into two parts, flow solver errors and regression modeling errors. The flow solver errors include the choice of governing equations, turbulence modeling, boundary conditions, numerical noise such as round-off error, degree of

convergence/averaging and discretization errors. The regression modeling errors are caused by a lack in polynomial approximation. By using second-order RSM, the regression model is written as

$$y = \beta_0 + \sum_{i=1}^{k} \beta_i x_i + \sum_{i=1}^{k} \beta_{ii} x_i^2 + \sum_{i<j} \sum_{j=2}^{k} \beta_{ij} x_i x_j + \epsilon \tag{4.2}$$

where βs are the regression coefficients, x_i is the i^{th} design parameter and k is the total number of design parameters. By minimizing the error using least-square fit of the regression coefficients, the approximation of the true response $\hat{y}$ is

$$\hat{y} = b_0 + \sum_{i=1}^{k} b_i x_i + \sum_{i=1}^{k} b_{ii} x_i^2 + \sum_{i<j} \sum_{j=2}^{k} b_{ij} x_i x_j \tag{4.3}$$

The bs are now the least-square estimators of the regression coefficients.

Some statistical coefficients are calculated to check the quality of the estimated regression model. The coefficient of multiple determination (R^2) and the adjusted one (R^2_{adj}) defined in equation 4.4 and 4.5 are measures of the variability of the model using the regressor variables $x_1, x_2, x_3, ..., x_k$. $R^2_{adj} = 1$ corresponds to perfect fit. The difference between R^2 and R^2_{adj} is that R^2 increases if a regressor is added to the model despite the fact that the added regressor will not improve the model; R^2_{adj} will however decrease. In order to increase the model fit and thus R^2_{adj}, it is possible to check the individual regressors using test statistics and reject the ones that do not fulfill a prescribed criterion. R^2 and R^2_{adj} are defined as

$$R^2 = 1 - \frac{SS_E}{SS_T} \tag{4.4}$$

$$R^2_{adj} = \frac{1 - SS_E/(n-p)}{SS_T/(n-1)} \tag{4.5}$$

$SS_E = \sum_{i=1}^{n} (y_i - \hat{y}_i)^2$ is the sum of square of errors, $SS_T = \sum_{i=1}^{n} (y_i - \bar{y})^2$ is the total sum of square, n is the number of observations, p is the number of regressors, y_i is the i^{th} observation, $\hat{y}_i$ is the i^{th} predicted value and $\bar{y}$ is the mean value.

The residuals and the studentized residuals (r_i) are analyzed to check outliers. The studentized residuals (eq. 4.6) are obtained by

scaling the residuals in such a way as to obtain the constant variance of each residual $Var(r_i) = 1$. Outliers have been removed if $|r_i| > 3$.

$$r_i = \frac{\hat{\epsilon}_i}{Var(\hat{\epsilon}_i)}, \text{ where } \hat{\epsilon}_i \text{ is the } i^{th} \text{ error, } \hat{\epsilon}_i = y_i - \hat{y}_i \tag{4.6}$$

4.2 Design of Experiments

It is important to choose appropriate values of the parameters for each design candidate. The method of the statistically appropriate choice for best fit is called "Design of Experiment" (DOE). There are many DOE methods for second-order models and deciding which one to choose is problem dependent. There are e.g. central composite design (CCD), spherical CCD, Box Behnken design and face-centered central composite design. Each design has specific advantages/disadvantages with respect to the problem at hand. The design chosen is the face-centered central composite design shown in figure 4.1(a). The boundary constraints of the design space are defined by upper and lower values for each parameter. These are normalized to $+1$ and -1 respectively.

The optimization parameters must be chosen with care and must be as few as possible. Figure 4.1(b) shows the number of required designs versus the number of parameters. The number of designs is $2^k + 2k + 1$, where k is the number of parameters.

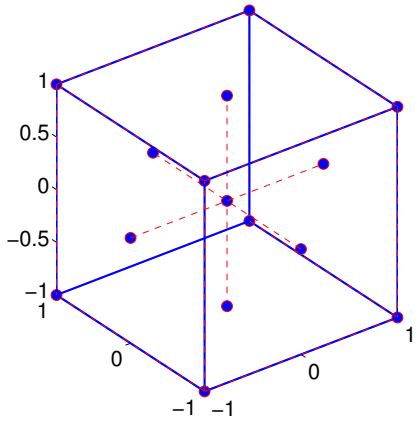

(a) Face-centered central composite design, DOE for RSM. The blue line is the boundary of the design space.

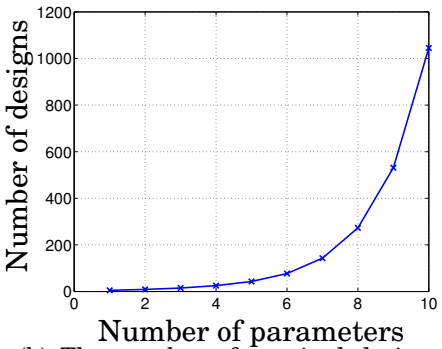

(b) The number of required designs versus parameter space.

Chapter 5

Summary of Results

This chapter gives a brief summary of the results reported in the seven appended papers on which this thesis is based. The scope of the work has been to evaluate the potential of AFC on truck-trailers. Numerical, experimental and full-scale road tests have been investigated.

5.1 Paper I

5.1.1 Motivation and Background

The reader may wonder what the relation is between tilt-rotor aircrafts and truck-trailers. The thesis starts with a method verification and analysis study of a similar well known AFC case experiment of a tilt-rotor wing with a successful full-scale test. Not much information is given about tilt-rotor aircraft but a short summary of their functions and benefits is offered here. The tilt-rotor aircraft has many benefits in comparison with a helicopter. These include speed, range and payload. It has the helicopter's capabilities of vertical take-off and landing as well as the cruise speed, range and fuel economy of a fixed-wing aircraft. The main idea is that, during take-off, the prop-rotors with their engines are positioned with the axis vertical, like those of a helicopter, in order to achieve vertical propulsive lift. At a desired height, the prop-rotors are tilted successively horizontally towards conventional propeller airplane position where the lift capability is moved from the prop-rotors to the wings, and hence the cruise speed, range and fuel economy are improved. Research on tilt-rotor aircrafts began in 1940. The XV-3 was built in 1953 as a prototype for future improvements. Development of XV-15 started in 1972 and was funded by NASA, the U.S. army and Bell Helicopter Textron. The experience gained from these two was applied in 1981 in construction of the V22. The main

drawback of tilt-rotor aircraft is that, during hover, the rotors create an airstream that impinges on the wing and a part of the fuselage. This yields a significant loss of lift capability. This loss, or download, is estimated to be 10% of the weight of the aircraft and almost equal to the V-22 capability in terms of payload. To reduce this download, NASA, Bell and Boeing started a research project on flow around a wing during hover. The result was a wing with a deflected flap that reduced the area exposed to the airstream and narrowed the wake. In optimization terms, the flap deflection should be increased from its optimum, but the airstream would separate and hence the download would increase. In this state, AFC is the solution. With AFC, the flow re-attaches, the wake becomes narrower and the download is alleviated. The method used in this paper is numerical, and large-eddy simulation (LES) is adopted. The numerical results in Paper I are in good agreement with the experiment, and a good understanding of the mechanism of AFC is developed.

5.1.2 Work and Results

The wing investigated has a deflected flap at the trailing edge. The optimal angle is 70°, where the flow re-attaches. If the deflection angle is increased, the flow separates and hence the download increases. With active flow control (AFC), the results show that the flow reattaches, the wake becomes narrower and the download is alleviated. The spatial discretization scheme dependence was also investigated. For the blended scheme, the blending factor chosen was 0.95, i.e. 95% CD and 5% UD.

The predicted drag for the unforced case is in good agreement with experimental results and previous FEM computations, (Kjellgren *et al.*, 2002*b*,*a*). The normalized drag for the unforced case is 0.99. The experimental value is 1.03, (Kjellgren *et al.*, 2002*b*). This is the case for the pure CD scheme; however, this scheme showed wiggles in the region upstream of the wing. The MARS scheme over-predicted the drag as 1.52, and the blended CD scheme also over-predicted it as 1.27. These two latter schemes however removed the wiggles. The predicted drag for the forced case is also in good agreement with the experimental results and previous FEM computations. The normalized drag is 0.76 for the pure CD scheme, compared with the experimental value of 0.73, (Kjellgren *et al.*, 2002*b*). We did not run the forced case with the MARS scheme due to the high over-prediction of the unforced case. However, for the blended scheme, the normalized drag is 0.84. The results below were all obtained with the blended scheme. In the drag and lift his-

tory plots in Figure 5.1, we can see that there are large fluctuations for the unforced case and that the peak to peak value is reduced with forcing. Figures 5.2(a) and 5.2(b) show contour plots of the time aver-

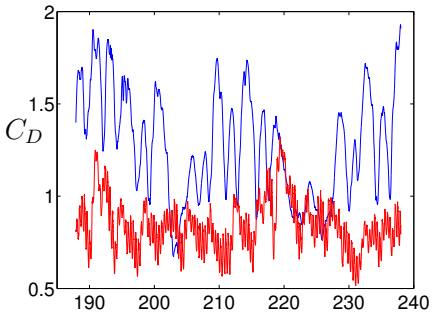

(c) Normalized drag history.

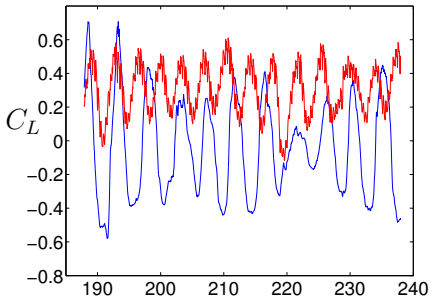

(d) Normalized lift history.

Figure 5.1: Time histories of drag and lift, —— : AFC OFF; —— : AFC ON.

age of the x-component of velocity together with streamlines. For the unforced case, we observe a large separation region along the flap and a large wake region. We also observe that there is a large region with negative velocities (dark blue) behind the wing in the unforced case. With AFC, the large separation on the flap region is removed (i.e. the time-averaged flow is re-attached), the wake size narrows a great deal and the region with negative velocities behind the wing is smaller. The wake structures become smaller.

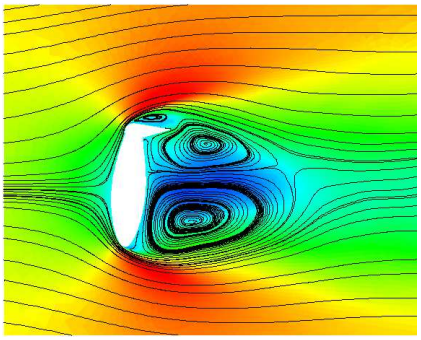

(a) Mean U-velocity, AFC OFF.

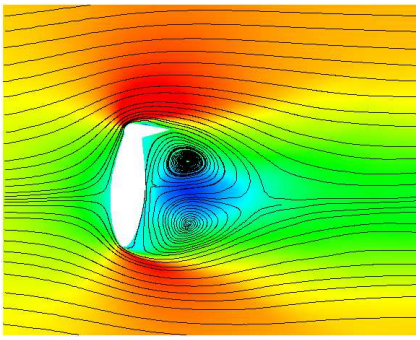

(b) Mean U-velocity, AFC ON.

Figure 5.2: Mean U-velocity and streamlines.

5.1.3 Comments

The purpose of this paper is to evaluate a method which will be used in our research on truck-trailers. The choice of the STAR-CD code was based on efficient knowledge transfer and for practical purposes, since this code was widely used at Volvo 3P and Volvo Technology. The computational mesh lacks slightly in quality for LES, although the results are in good agreement with experiments.

5.2 Paper II

5.2.1 Motivation and Background

The lessons learned from the tilt-rotor study were applied and defined our initial research strategy for drag reduction on trucks. A large number of LES computations were carried out, investigating the possibility to reduce the drag by using active flow control.

5.2.2 Work and Results

The truck is simplified as a rectangular bluff-body with a typical width ($w = 2.6\ m$) and length ($l = 13.0\ m$) relevant for a real truck and an appropriately large slice is chosen in the third direction (height), see figure 3.1. The truck is mounted with angled flaps on the rear end in which the oscillating synthetic jet actuators are placed. The actuators are modeled as a time varying boundary condition (slot). The slot extends over the entire height (z) of the truck. It was found that a reduction of the drag by up to 25% was possible for certain configurations. A thorough analysis of the mechanism of flow control and the flow characteristics of the forced and unforced case was reported.

Figure 5.3 plots the time-averaged streamlines. It is clear that the wake structure is affected in the forced case. The smaller wake structure of the forced case can be seen in figure 5.3(b). The wake is narrower and has a shorter distribution in the free stream direction. It is clear that the time-averaged flow is entirely re-attached on the flap surface by active flow control. Furthermore, in the unforced case, flow comes from the back side of the truck, up to the flap surface. In the forced case, this flow is prevented by the re-attached streamlines. This is one of the reasons why the interaction of the lower and upper shear layers is prevented.

Figure 5.4(a) plots the drag history for the forced and the unforced cases. It is clear that the forced case has lower drag at every instant

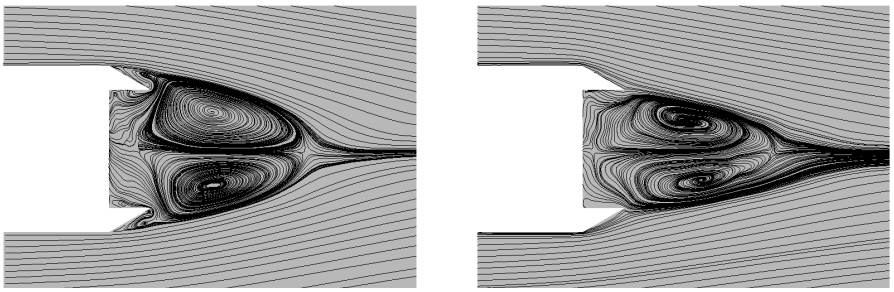

(a) AFC OFF (b) AFC ON

Figure 5.3: Time-averaged velocity streamlines, zoom of the wake.

when the flow has reach fully developed conditions. Figure 5.4(b) plots the power spectral density of the drag signal. We notice the vortex shedding frequency in both the unforced and forced cases with one difference. The peak of the forced case is reduced compared to the unforced case. The peaks are located at frequency $0.98\ Hz$, which corresponds to a Strouhal number of $St = 0.1$. This is in good agreement with measurements made on rectangular cylinders, (Okajima, 1982). In Okajima (1982), the author measured the Strouhal number of rectangular cylinders of different B/H as a function of Reynolds number. The Strouhal number was $St = 0.12$ for $Re = 2 \cdot 10^4$ and $B/H = 4$. The present truck model has $B/H = 5$ at $Re = 2 \cdot 10^5$. We further notice the high peak at $10\ Hz$ that corresponds to the actuation frequency. The intensity of the peak is high and, for this reason, there is high RMS drag of the forced case in figure 5.4(a).

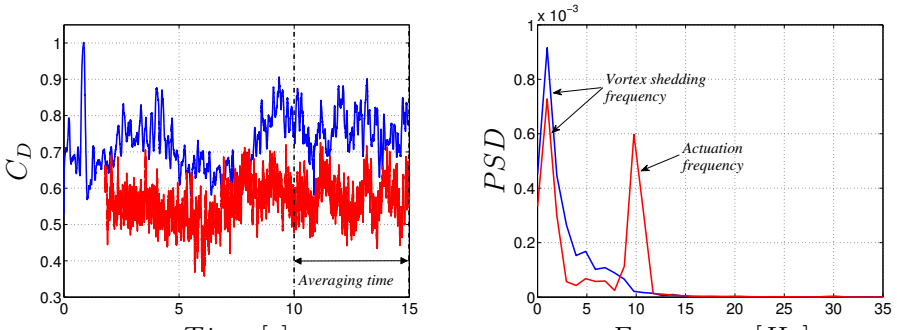

(a) Drag history (b) Power spectral density

Figure 5.4: Drag history and its FFT, —— : AFC OFF; —— : AFC ON. $C_D^{AFC\ OFF} = 0.76$**;** $C_D^{AFC\ ON} = 0.57$**. One time unit,** w/U_∞**, corresponds to** $0.1\ s$**.**

5.2.3 Comments

In this paper we used another simulation code, FlowPhys, than the code used, Star-CD, in Paper I. The reason was high fluctuations in drag history and pressure field when AFC was applied as BC for the truck model in Star-CD. No conclusions were made about the source of the fluctuations at that time (although later, in paper VII). The FlowPhys code was referred to as the FEM code with which the results were partly compared in Paper I. Another reason for the code change is that FlowPhys was faster than Star-CD in computing the turbulent flow with LES. The time-averaged flow shows slight asymmetry. Our first thought was that the time-averaged period had to be increased, but we found later that there was an error in one velocity component in the lower boundary condition for the AFC jet. That error was corrected in the following research.

5.3 Paper III

5.3.1 Motivation and Background

The promising numerical results of Paper II led to further research and evaluations for the repeatability of the drag reduction in full-scale tests and experiments. AFC requires a reliable and sufficiently powerful synthetic jet actuator. There are a large number of sophisticated synthetic jet actuators; a simple one was developed and experimentally evaluated.

5.3.2 Work and Results

The actuator consisted of a rectangular wood cavity, loudspeaker and an aluminum plate with a slot in the middle, see figure 3.10. The experiment investigated different slots and cavity volumes and reported the corresponding velocity profile and maximum velocity out from the slot. This actuator was similar to the one used in the tilt-rotor experiments and full-scale tests. Results show that the output velocities and corresponding momentum from the actuator were in the same order of magnitude as the requirements concluded from the computational study. Figure 5.5 shows the maximum and corresponding C_μ versus different slot widths.

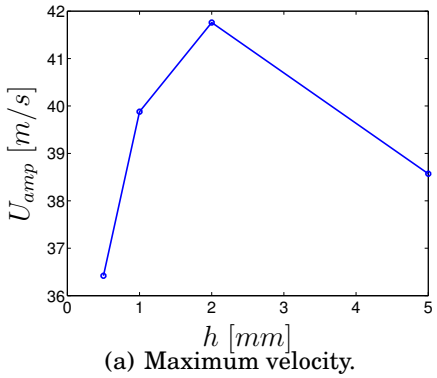

(a) Maximum velocity.

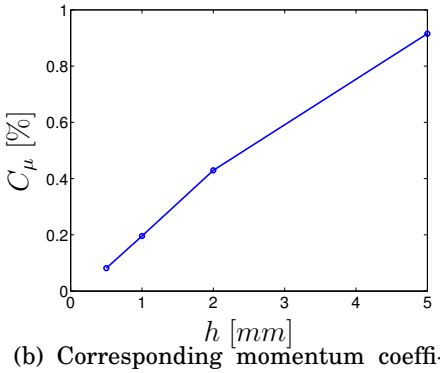

(b) Corresponding momentum coefficient.

Figure 5.5: Maximum velocity and C_μ with different slot width.

5.3.3 Comments

The choice of this actuator type was mainly based on limitations in time and its rather primitive implementation for full-scale road tests. This part of the study focused on high C_μ at low frequencies. A frequency study of the different loudspeakers was carried out but was unfortunately not completely reported. A part of this study is however found in Figure 10 in the paper. It was shown that the loudspeakers performed best at the corresponding resonance frequency, which was different for loudspeakers. The computations in Paper II show that low frequency is favorable. The choice of loudspeaker was based on both its overall performance as well as its performance at lower frequencies. The OFM of this actuator was not reported in the paper but later calculated to be ~ 0.1; compared with the actuator used in the successful XV-15 full-scale test, (McVeigh *et al.*, 2004), with $OFM = 0.015$, the current actuator is good.

5.4 Paper IV

5.4.1 Motivation and Background

The work progressed with full-scale investigations of a Volvo prototype vehicle, see figure 3.12. The trailer was mounted with three flaps at the rear sides and top end. The actuators were manufactured using the experience gained in Paper III; they were integrated in the flaps and connected to amplifiers that were supplied with a frequency generator controlled by LabView.

5.4.2 Work and Results

The full-scale test included passive and active flow control investigations by varying the flap angle, with and without AFC, investigating different frequencies and slot angle configurations. The test shows a fuel reduction of about 4% in a comparison of two flap angles. The test of active flow control shows a reduction of 5.3% compared to the corresponding unforced case with flaps. Compared with the baseline case, the passive flow control fails to reduce the total fuel consumption. The two-dimensional velocity profile out from the integrated actuators at two different slot angles is plotted in figure 5.6.

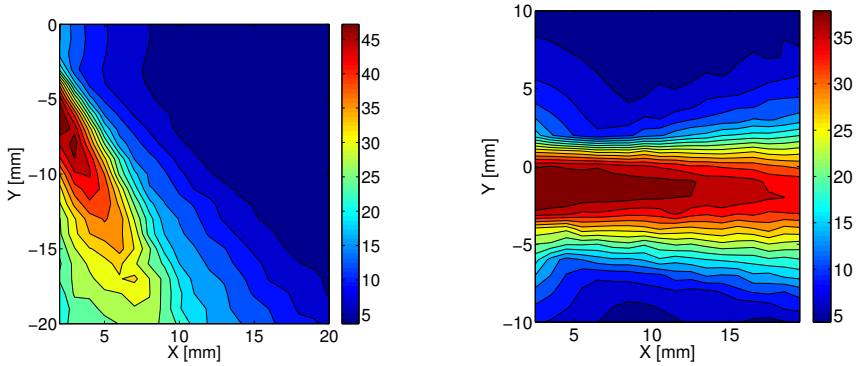

(a) $45°$ *slot angle* (b) $90°$ *slot angle*

Figure 5.6: Contour plots of phase averaged velocities at maximum velocity during the ejection stroke at two slot angles: $45°$ **and** $90°$**.**

The ratios of total consumed fuel by the test vehicle to the baseline case (case 10) are shown in table 5.1. The table includes full specifications of the test cases. A comparison between the unforced (no AFC) Case 2 with a flap angle of $30°$ and the corresponding forced (AFC) Case 4 shows a reduction of 5.4%. We also observe that, by using a smaller flap angle of $20°$ and no AFC (Case 3), the reduction is 4.3%. The reduction as compared to Case 2 is almost as large as the reduction gained in the forced case (Case 4). Comparing all cases with regard to frequencies, one can conclude that the highest frequency gives a slight improvement in the reduction of drag, e.g. comparing Case 1 and Case 4. Baseline case 10 has better fuel consumption than both passive Cases 2 and 3. The reason is probably that there is no flap on the lower edge of the trailer.

Case	AFC	FA	SA	Freq.	Ratio	Difference
1	ON	30	45	16.7	101.1%	+1.1%
2	OFF	30	–	–	105.0%	+5.0%
3	OFF	20	–	–	100.7%	0.7%
4	ON	30	45	23.3	99.6%	-0.4%
5	ON	30	90	16.7	102.7%	+2.7%
6	ON	30	90	23.3	102.3%	+2.3%
7	ON	20	90	16.7	99.5%	-0.5%
8	ON	20	90	23.3	99.5%	-0.5%
9	ON	30	Large slot	16.7	101.9%	+1.9%
10	Baseline	–	–	–	100.0%	0.0%

Table 5.1: Full-scale test cases specifications and results, rows colored light blue: unforced; and light red: forced. FA denotes Flap Angle and SA denotes Slot Angle.

5.4.3 Comments

There were some limitations from the manufacturing point of view that were not highlighted in the paper. Figure 5 in the paper shows that the slot should be as close as possible to the flow separation location. Unfortunately, it was not possible to manufacture this, but the closest possible location of the actuators to the flap hinge was implemented. This issue may be one of the reasons for the lack in full-scale performance of AFC.

5.5 Paper V

5.5.1 Motivation and Background

The failure to reduce the total fuel consumption with passive flow control led to further investigations using full 3D modeling with detached eddy simulation and an AFC experiment on the $1/10^{th}$ scale of a Volvo truck with fully detailed cab with simplified underbody and wheel housing, see figure 3.4 . This work was carried out as a bachelor thesis project (Andersson *et al.*, 2011), supervised by the authors in the Paper.

5.5.2 Work and Results

The failure of the passive flow control was recovered neither by the experiment nor in the DES computations. Rather, the experiments and

computations demonstrated that the AFC works successfully and results in flow re-attachment to the flaps. The drag reduction was about 3-4%. Table 5.2 shows the time-averaged drag values for the simulations and experiments.

Configuration	C_D Exp	ΔC_D Exp [%]	C_D DES	ΔC_D DES [%]
Baseline	0.53	-	0.55	-
PFC	0.52	-1.77	0.54	-0.66
AFC	0.51	-3.13	0.53	-3.96

Table 5.2: Table 3: Experimental and numerical drag values of different configurations.

Figure 5.7 depicts the difference between the PFC and AFC flow field. The tufts at the trailing edge of the trailer for the PFC case (Figure 5.7(a)) are non-uniformly oriented. This is due to the separated flow region. During the experiment, the tufts at the flap trailing edge were also randomly moving, which showed the effect of the strong vortex shedding. The AFC case in Figure 5.7(b) has streamlined tufts at all places. This shows that the AFC evidently succeeded in re-attaching the separated flow. During the experiment, it was noticed that the flow re-attached immediately when AFC was set on. Figure 5.8 shows the

a)  b) 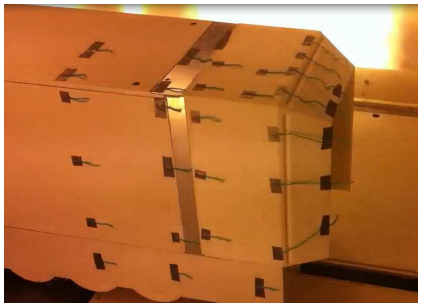

Figure 5.7: Flow visualization by tufts in the wind tunnel, PFC (a) and AFC (b).

DES streamlines of x-velocity in different views. These also confirm the narrower and shorter wake size of the AFC configuration compared to the PFC one. It is noticeable that the lower dead region in the wake of the PFC configuration (figures 5.8(a) and 5.8(c)) is alleviated by the AFC (figures 5.8(b) and 5.8(d)).

5.5.3 Comments

The drag reduction numbers in the conclusions in Paper V are incorrect, the correct are found in table 3 in the paper and repeated here: the

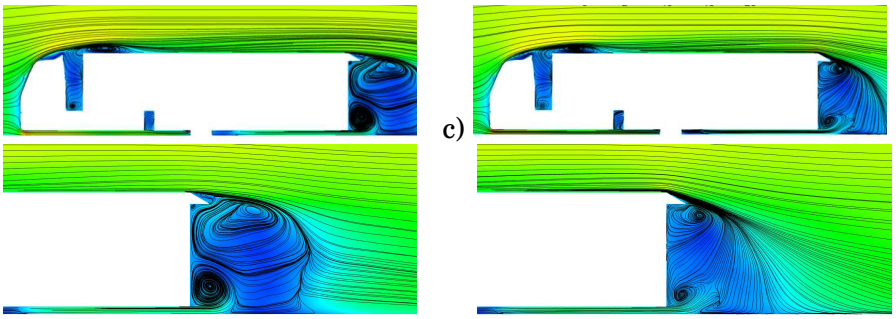

Figure 5.8: Contours of time-averaged x-velocity and streamlines x-z view (symmetry plane): PFC (a) and (c) and AFC (b) and (d) configurations.

numerical simulations show that the drag coefficient, C_D, decreased by 4.0% when AFC was activated compared to the baseline case without flaps. The corresponding decrease when AFC was deactivated is only 0.7%. The experimental results show a decrease in C_D of 3.1% for the case in which AFC was activated compared to the baseline case. With AFC deactivated, the corresponding decrease in C_D was 1.8%.

5.6 Paper VI

5.6.1 Motivation and Background

The flap geometry had not yet been considered until this point and was chosen to be as simple as possible, i.e. a straight flap with a defined length and flap angle. The modest reduction in drag in the fully 3D model, which was used in the experiment and DES computation, opened for optimization studies of the flap shape and some major AFC parameters. The response surface methodology was adopted as the optimization strategy.

5.6.2 Work and Results

Results suggest a curved flap shape. Table 5.3 gives the parameter values that correspond to this minimum in drag, and figure 5.9 shows the geometry and mesh. The drag value from the optimization is however in less good agreement with LES made on this configuration.

Parameter	Value
Flap angle α	$30°$
1^{st} flap coord y_1	$0.10\ m$
2^{nd} flap coord y_2	$0.015\ m$
Slot angle β	$15\ deg$
Slot position X_f	$0.3\ \%$

Table 5.3: The proposed optimized case by the improved response surface model for drag.

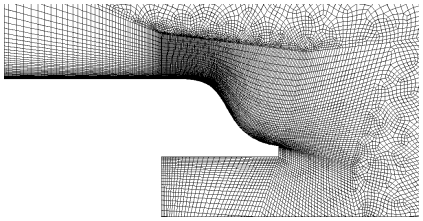

Figure 5.9: The geometry and mesh of the proposed optimized case by the response surface model for drag.

5.6.3 Comments

The optimization is dependent on how the flap is connected to the truck rear end. Several efforts were carried out to optimize the flap geometry with a sharp edge between the rear end of the truck and the flap but the optimization proposed straight flap. The smooth connection is crucial for curved geometry. The optimized flap geometry would have been run with the 3D geometry but this is postponed to future works.

5.7 Paper VII

5.7.1 Motivation and Background

The thesis concludes with a numerical modeling study of active flow control. The work compares different CFD codes and evaluates the modeling aspect of flow control.

5.7.2 Work and Results

It is found that, for incompressible FVM codes, the pressure field oscillates with time, synchronized with the periodic oscillating flow control boundary condition, whereas, for incompressible FEM and compressible FVM codes, the pressure field in the domain is stable. The pressure

at three different time instants in the forcing period is plotted in figure 5.10. The times when the pressure is close to maximum, zero and minimum occur at zero, minimal and second zero forcing in the forcing suction period are indicated in figure 5.10(a). The differences between the codes are remarkable. FlowPhys and STAR-CCM+ compressible show stable pressure fields at all three time instants. Both Fluent and STAR-CCM+, i.e. the incompressible FVM codes, show large differences in pressure in the whole domain at the three time instants.

5.7.3 Comments

The results invite for further research in of AFC modeling and emphasize the sensitivity of the FVM incompressible codes to abrupt changes in pressure elsewhere in the domain.

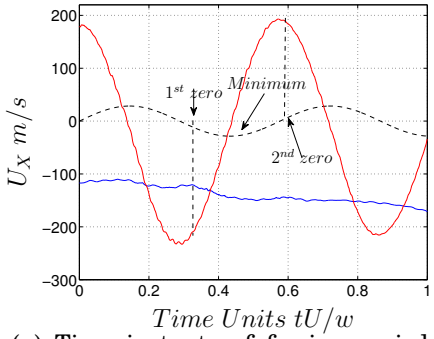

(a) Time instants of forcing period. (——) unforced and (——) forced case. (- - -) forcing at the slot

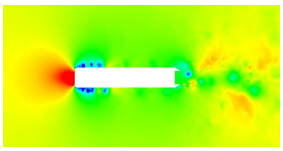

(b) FlowPhys: 1^{st} zero AFC

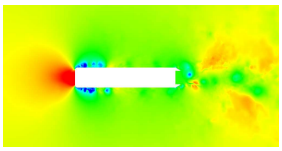

(c) FlowPhys: min AFC

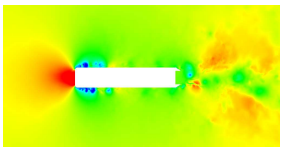

(d) FlowPhys: 2^{nd} zero AFC

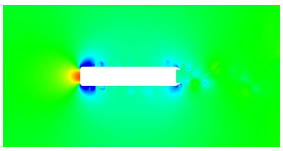

(e) Fluent: 1^{st} zero AFC

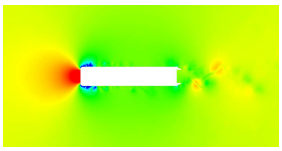

(f) Fluent: min AFC

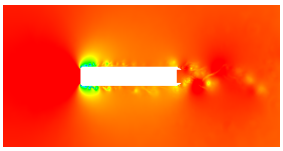

(g) Fluent: 2^{nd} zero AFC

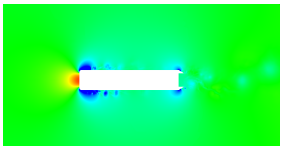

(h) CCM: 1^{st} zero AFC

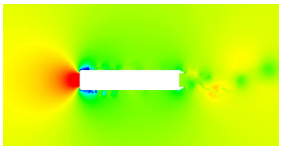

(i) CCM: min AFC

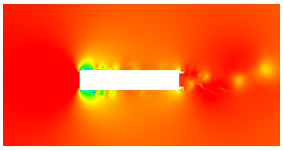

(j) CCM: 2^{nd} zero AFC

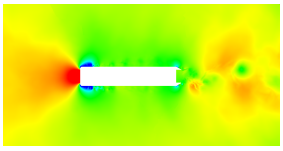

(k) CCM compressible: 1^{st} zero AFC

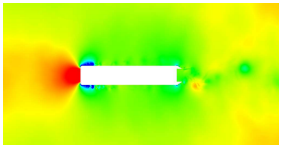

(l) CCM compressible: min AFC

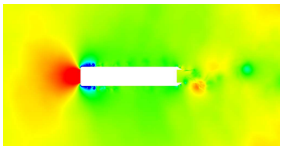

(m) CCM compressible: 2^{nd} zero AFC

Figure 5.10: Time series of the pressure field in the $x-y$ plane around the truck in different codes, $red > 200Pa$, $blue < -500Pa$ and identical colorbar for all figures.

Chapter 6

Concluding Remarks

ACTIVE flow control techniques have been investigated for truck-trailers. This chapter summarizes the most important conclusions of the flow physics and research methods. The chapter concludes with proposals for future work.

6.1 Flow physics

Flow re-attachment of the separated flow on the flaps is achieved by AFC. This was shown in the computations in Paper II and experiment in Paper V. The instantaneous characteristics of the unforced case were found to be typical of bluff body flows, with strong global vortex shedding and reversed flow on the flaps. The forced case has weaker vortex shedding, and the separated flow was reattached on the flaps.

Small vortices were observed on the flap surface that were created by the actuation. These vortices move downstream of the flap surface, creating a shear layer in the wake that prevents interaction between the naturally created shear layers on the upper and lower edges.

Pressure recovery in the wake of bluff-body flow was observed that was due to AFC. The unforced cases had large time-averaged low pressure regions in the wake and on the flap surface. The time-averaged pressure in the wake of forced cases was considerably higher.

RMS of pressure was greatly suppressed in the wake owing to AFC, which decreases the level of vortex shedding in the wake and

makes the wake less intensive. The RMS of pressure was increased on the flap surface with actuation, however, which created a strong low pressure region at the leading edge of the flap that makes the flow stay attached.

A narrower wake size was observed. The wake also had a shorter distribution in the streamwise direction due to AFC. This was observed in all computations. A shorter wake size yields higher pressure and explains the reduction in drag of the vehicle.

Drag reduction of different magnitudes was achieved. The low drag of the forced case is due to the increased base pressure at the rear end of the truck that was shown by the C_p analysis.

The influence of slot angle is important for drag reduction. Smaller slot angles are preferable. The phase-locked flow at two different slot angles was analyzed, and it was shown that the improved ability to reduce drag of small slot angles has to do with the dynamics of the AFC around the flap region. Two vortices per cycle were created by the actuation for the smaller slot angle case (Case A) compared to one vortex per cycle for the larger slot angle case (Case B). The flow in Case A smoothly re-attached upstream of the vortices that were created, which were significantly smaller and had a faster movement than the vortex in Case B. The time-averaged pressure was also investigated for both cases, and it was shown that the base pressure in Case A is larger than that in Case B, as expected.

6.2 Research Methods

A simplified semi-3D truck model approach was good for physical analysis comparing the unforced and forced cases. The simulation time was manageable, although the turbulent flow was computed using LES. The amount of drag reduction in these models was not fully repeatable in the experiment or full-scale test. The spanwise domain and mesh resolution were also investigated in (El-Alti, 2009). The RMS of the drag was decreased with a larger size of the spanwise domain and lower mesh resolution. The flow becomes more two dimensional when the domain size is small, and the three dimensionality and the effect of AFC are much more clear in large domains. The drag reduction achieved is consistent with different spanwise domain sizes.

The actuator concept used in the experiments and full-scale tests had the capability to produce desired output velocities and momentum. It was shown that a C_μ of 1% and velocities up to $U_p = 40m/s$ was possible. Further, it was shown that the cavity volume did not have any effect on the maximum velocity achieved. This is desirable when manufacturing the device for the full-scale test. The actuator was more suited to an experimental enviroment than a full-scale road test due to the complications of power supplies and heating inside the trailer, which affected the amplifiers.

The experimental scale model showed the potential of AFC for a more realistic truck-trailer taking into account 3D effects and characteristic details of truck-trailers. The model was a semi-detailed Volvo truck-trailer. The experiment and DES were in good agreement. The drag reduction achieved was smaller compared to semi-3D truck model.

The full-scale test showed the importance of passive devices that may negatively affect the drag of the truck-trailer. The effect of AFC was observed to a give a magnitude of 5% fuel reduction compared to the corresponding unforced PFC case, but the total fuel consumption compared to the baseline case (i.e. without any flaps) was not reduced with either passive case.

The combined research methods of LES, experiments, DES and full-scale road test are of great importance. Each research method has its advantages and disadvantages. The different research methods complements one another and promote different perspectives of aerodynamics research to make it more applied and robust.

6.3 Additional conclusions

Response surface methodology demonstrated that the choice of optimization strategy is of great importance, especially when simulations are time-consuming. For LES, the surrogate model optimization approach is ideal due to the possibility of simultaneous simulations of design candidates. The present results indicate, a region of feasible designs. The flap angle, α, has its optimum at 30° and a slot angle as low as possible. The slot position is highly dependent on the proposed flap shape. The poor agreement of the response surface model results with the value predicted by LES may have several possible causes. The design space is probably

too wide, and running LES in general produces highly unsteady turbulent flow fields that are sensitive to averaging times, mesh quality and fluctuations in the central difference scheme.

Oscillations in the pressure field in the entire domain are encountered in incompressible FVM code when forcing is applied at a small slot on the truck. The compressible and incompressible FEM code show an invariant and stable pressure field when the forcing is applied. The prediction in drag for both the unforced and forced cases in incompressible FVM codes are in agreement. There is a minor difference in the prediction of drag comparing compressible and incompressible FVM codes. The drag values are in good agreement in comparisons of the incompressible FEM and the compressible FVM codes. The amount of reduction in drag between the forced and unforced cases varied between ~ 20 and 30%.

6.4 Future Work

Optimization using RSM with fewer parameters and with a more confined design space in order to improve the agreement of the proposed optimized design with LES results.

DES of or experiments on the proposed optimal case by RSM to investigate the potential of higher drag reduction. If high drag reduction is achieved, a full-scale test should be prepared.

Improve the actuator concept for the full-scale test by including transitional ducts that smoothly guide the flow from the loudspeaker to the actuator slots as in the experimental scale model or use other types of actuators that are more robust at road conditions.

Investigate passive flow control devices more thoroughly both with semi-3D and full 3D simulations. The potential of PFC is important due to its easier and more practical installation.

Bibliography

ANDERSSON, E., ANDERSSON, E., GRANSTRÖM, B., LÖFGREN, N., NYBERG, N. & SVEDMAN, J. 2011 Aktiv strömningskontroll av vaken bakom en lastbil: Ett försök att minska bränsleförbrukningen hos lastbilar. *Tech. Rep.*. Div. of Fluid Dynamics, Dep. of Applied Mechanics, Chalmers University of Technology, Göteborg, Sweden.

ARWATZ, G., FONO, I. & SEIFERT, A. 2008 Suction and oscillatory blowing actuator modeling and validation. *AIAA Journal* **46** (5), 1107–1117.

BARNARD, R. H. 2001 *Road Vehicle Aerodynamic Design*, 2nd edn. Mechaero Publishing.

BUCKLEY JR., F. & MARKS, C. 1979 Feasibility of active boundary-layer-control methods for reducing aerodynamic drag on tractor trailer trucks. *Journal of Industrial Aerodynamics* **4** (2), 133–148.

CATTAFESTA, L. & SHEPLAK, M. 2011 Actuators for active flow control. *Annual Review of Fluid Mechanics* **43**, 247–272.

CHOI, H., JEON, W.-P. & KIM, J. 2008 Control of flow over a bluff body. *Annual Review of Fluid Mechanics* **40**, 113–139.

COLLIS, S., JOSLIN, R., SEIFERT, A. & THEOFILIS, V. 2004 Issues in active flow control: Theory, control, simulation,' and experiment. *Progress in Aerospace Sciences* **40** (4-5), 237–289.

DARABI, A. & WYGNANSKI, I. 2004 Active management of naturally separated flow over a solid surface. part 1. the forced reattachment process. *Journal of Fluid Mechanics* **510**, 105–129.

DAVIDSON, L. 2011 *Fluid mechanics, turbulent flow and turbulence modeling*, 1st edn. Chalmers University of Technology.

DOYLE, J., HARTFIELD, R. & ROY, C. 2008 Aerodynamic optimization for freight trucks using a genetic algorithm and cfd. In *46th AIAA Aerospace Sciences Meeting and Exhibit*.

EL-ALTI, M. 2009 Active Flow Control for Aircrafts and Heavy Vehicles. Thesis for licentiate of engineering no. 2009:011. Div. of Fluid Dynamics, Dept. of Applied Mechanics, Chalmers University of Technology, Göteborg, Sweden.

EL-ALTI, M., KJELLGREN, P. & DAVIDSON, L. 2008 On the download alleviation for the XV-15 wing by active flow control using large-eddy simulation. In *ERCOFTAC Workshop: Direct and Large-Eddy Simulation 7*. Trieste, Italy.

EL-ALTI, M., KJELLGREN, P. & DAVIDSON, L. 2009 Drag reduction of trucks by active flow control of the wake behind the trailer. In *6th International Symposium on Turbulence, Heat and Mass Transfer*. Rome, Italy.

ENGLAR, R. J. 2005 Improved pneumatic aerodynamics for drag reduction, fuel economy, safety and stability increase for heavy vehicles. In *SAE 2005 Commercial Vehicle Engineering, Congress and Exhibition*. SAE Paper 2005-01-3627, Chicago, Illinois, USA.

EU 2012 Mer konkurrenskraftiga och resurseffektiva transporter.

GAD-EL-HAK, M. 2000 *Flow Control: Passive, Active and Reactive Flow Management*. London, United Kingdom: Cambridge University Press.

GAD-EL-HAK, M. & POLLARD, A. 1998 *Flow Control: Fundamentals and Practices*. Germany: Springer-Verlag Berlin Heidelberg.

GEORGE, W. K. 2006 *Lectures in Turbulence for the 21st Century*, 1st edn. Chalmers University of Technology.

GLEZER, A. & AMITAY, M. 2002 Synthetic jets. *Annual Review of Fluid Mechanics* **34**, 503–529.

GREENBLATT, D. & WYGNANSKI, I. 2000 Control of flow separation by periodic excitation. *Progress in Aerospace Sciences* **36** (7), 487–545.

HENNING, L. & KING, R. 2005 Drag reduction by closed-loop control of a separated flow over a bluff body with a blunt trailing edge. In *44th IEEE Conference on Decision and Control and European Control Conference ECC 2005*, pp. 494–499. Seville, Spain.

HJELM, L. & BERGQVIST, B. 2007 European truck aerodynamics - a comparison between conventional and coe truck aerodynamics and a look into future trends and possibilities. In *The Aerodynamics of Heavy Vehicles II: Trucks, Buses and Trains*.

HUCHO, W.-H. 1998 *Aerodynamics of Road Vehicles*, 4th edn. Society of Automotive Engineers.

HYAMS, D., SREENIVAS, K., PANKAJAKSHAN, R., STEPHEN NICHOLS, D., ROGER BRILEY, W. & WHITFIELD, D. 2011 Computational simulation of model and full scale class 8 trucks with drag reduction devices. *Computers and Fluids* **41** (1), 27–40.

KJELLGREN, P., ANDERBERG, N. & WYGANSKI, I. 2000 Download alleviation by periodic excitation on a typical tilt-rotor configuration - computation and experiment. In *Fluids 2000 Conference and Exhibit*. Denver, CO.

KJELLGREN, P., CERCHIE, D., CULLEN, L. & WYGANSKI, I. 2002*a* Active flow control on bluff bodies with distinct separation locations. In *1st Flow Control Conference*. St. Louis, Missouri.

KJELLGREN, P., EL-ALTI, M. & DAVIDSON, L. 2009 Download alleviation of a tilt-rotor wing by active flow control strategies. In *KATnet II Conference: Key Aerodynamic Technologies*. Bremen, Germany.

KJELLGREN, P., HASSAN, A., SIVASUBRAMANIAN, J., CULLEN, L., CERCHIE, D. & WYGANSKI, I. 2002*b* Download alleviation for the XV-15: computations and experiments of flows around the wing. In *Biennial International Powered Lift Conference and Exhibit*. Williamsburg, Virginia.

LEUCHEN, J. & COOPER, K. R. 2007 Summary of full-scale wind tunnel tests of aerodynamic drag-reducing devices for tractor-trailers. In *The Aerodynamics of Heavy Vehicles II: Trucks, Buses and Trains*.

MCCALLEN, R., SALARI, K., ORTEGA, J., DECHANT, L., HASSAN, B., ROY, C., POINTER, W., BROWAND, F., HAMMACHE, M., HSU, T. *et al.* 2004 Doe's effort to reduce truck aerodynamic drag-joint experiments and computations lead to smart design. *Tech. Rep.*. Lawrence Livermore National Laboratory (LLNL), Livermore, CA.

MCVEIGH, M., KIEDAISCH, J., NAGIB, H., STALKER, A., WOOD, T. & WYGNANSKI, I. 2004 Model and full scale tiltrotor download reduction tests using active flow control. In *Annual Forum Proceedings - American Helicopter Society*, , vol. 1, pp. 24–32.

MYERS, R. H. & MONTGOMERY, D. C. 2002 *Response Surface Methodology: Process and Product Optimization Using Designed Experiments*. USA: A Wiley-Interscience Publication.

NAYERI, C. N., HAFF, J., GREENBLATT, D., LOEFDAHL, L. & PASHEREIT, C. O. 2007 Drag reduction on a generic tractor-trailer using active flow control in combination with solid flaps. In *The Aerodynamics of Heavy Vehicles II: Trucks, Buses and Trains*.

OKAJIMA, A. 1982 Strouhal numbers of rectangular cylinders. *Journal of Fluid Mechanics* **123**, 379–398.

ORTEGA, J., SALARI, K. & STORMS, B. 2009 Investigation of tractor base bleeding for heavy vehicle aerodynamic drag reduction. *Lecture Notes in Applied and Computational Mechanics* **41**, 161–178.

PANKAJAKSHAN, R., MITCHELL, B. & WHITFIELD, D. L. 2007 Full-scale simulations of drag reduction devices for class 8 trucks. In *The Aerodynamics of Heavy Vehicles II: Trucks, Buses and Trains*.

PANTON, R. 2005 *Incompressible Flow*, 3rd edn. Wiley.

PETROLEUM, B. 2012 BP statistical review of world energy.

R. BUZZ POWELL, B. J. G. & ROSENTHAL, B. 2009 Sae j1321 (tmc rp-1102) type ii fuel consumption test. *Tech. Rep.*. Program for Advanced Vehicle Evaluation PAVE, Auburn University.

SEIFERT, A. 2007 Closed-loop active flow control systems: Actuators. *Notes on Numerical Fluid Mechanics* **95**, 85–102.

SEIFERT, A., BACHAR, T., KOSS, D., SHEPSHELOVICH, M. & WYGNANSKI, I. 1993 Oscillatory blowing: A tool to delay boundary-layer separation. *AIAA Journal* **31** (11), 2052–2060.

SEIFERT, A., STALNOV, O., SPERBER, D., ARWATZ, G., PALEI, V., DAVID, S., DAYAN, I. & FONO, I. 2007 Large trucks drag reduction using active flow control. In *The Aerodynamics of Heavy Vehicles II: Trucks, Buses and Trains*.

SMITH, B. & GLEZER, A. 1998 The formation and evolution of synthetic jets. *Physics of Fluids* **10** (9), 2281–2297.

TAUBERT, L. & WYGNANSKI, I. 2007 Preliminary experiments applying active flow control to a 1/24th scale model of a semi-trailer truck. In *The Aerodynamics of Heavy Vehicles II: Trucks, Buses and Trains*.

UKIP 2012 Though tests for the volvo FMX.

Appendix A

Additional Results

A.1 Drag versus C_μ and F^+

This section is additional to chapter 3 in Paper II and investigates the influence of the frequency (figure A.1(a)) and the amount of momentum transfer (C_μ) of ejection and suction (figure A.1(b)) on the reduction of drag.

F^+ is the non-dimensional frequency, which is defined as

$$F^+ = f \cdot \frac{X_{TE}}{U_\infty} \tag{A.1}$$

C_μ is the amount of momentum out from the slot and is defined as

$$C_\mu = \frac{u_{RMS}^2 \cdot h}{\frac{1}{2} w \cdot u_\infty^2} \tag{A.2}$$

where h is the slot width, u_{RMS} is the RMS velocity from the jet and w a characteristic length used in the model in which AFC is applied. In this case, w is the width of a truck and the slot width is $h = 6\ cm$ (El-Alti *et al.*, 2009).

The range investigated at constant $C_\mu = 0.6$ is $0.3 \leq F^+ \leq 0.9$, which corresponds to Strouhal numbers of $\sim 1.0 - 3.1$ based on the width of the body. As the wake Strouhal number is 0.12, the actuation frequency is much higher than the vortex shedding frequency. It is found that the optimal actuation frequency is $F^+ = 0.5$ as regards to maximum reduction in drag. A wide range of C_μ is investigated at constant $F^+ = 0.3$ in order to study the maximum drag reduction that can be gained using AFC. As can be seen, the maximum drag reduction is at $C_\mu = 1.0\%$.

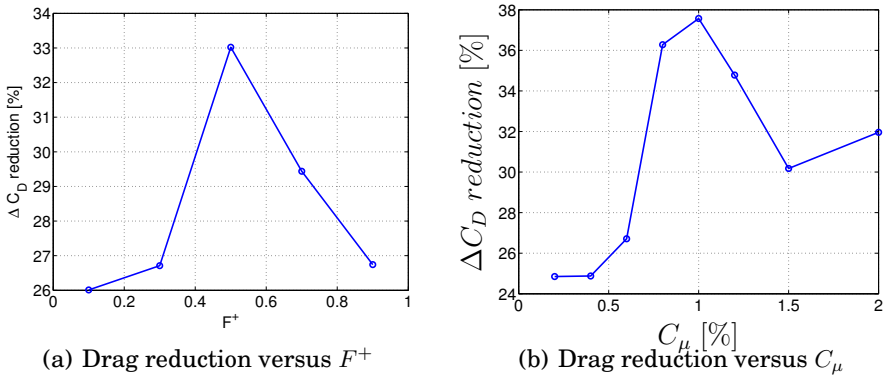

(a) Drag reduction versus F^+ (b) Drag reduction versus C_μ

Figure A.1: Drag reduction versus C_μ and F‘+.